UNIVERSIDADE DE LISBOA

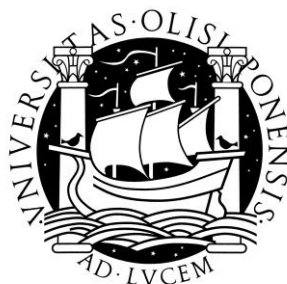FACULDADE DE CIÊNCIAS

DEPARTAMENTO DE QUÍMICA E BIOQUÍMICA

Copper compounds (Schiff bases) as DNA-Interacting Agents

Rosa Maria Faustino Brissos

Master of Science: Medical Inorganic Chemistry – Applications in Diagnosis and

Therapy

Lisbon

2011

UNIVERSIDADE DE LISBOA

FACULDADE DE CIÊNCIAS

DEPARTAMENTO DE QUÍMICA E BIOQUÍMICA

Copper compounds (Schiff bases) as DNA-Interacting Agents

Rosa Maria Faustino Brissos

Master of Science: Medical Inorganic Chemistry – Applications in Diagnosis and Therapy
Dissertation supervised by Prof. Doctor Patrick Gamez and Prof. Doctor Maria Helena Garcia.

Lisbon

2011

Acknowledgements

I would like to express my appreciation to two great women and excellent Professors Dr. Helena Garcia and Professor Dr. Virtudes Moreno for the excellent guidance, support and advice.

I would like to express my appreciation to my tutor and mentor Professor Dr. Patrick Gamez for all the trust, the support, encouragement, patience and the excellent guidance and advice. His continuous good mood and humor helped me and encouraged me in every moment.

I am so grateful to my Dream Team, my lab family, for all the support and all the help in every lab. Thanks André, Esther, Flavia, Jordi, Ibis, Alejandra Silvia, Andreu, Natalia, Shubhanch, Beltzane and all the great Inorganics.

I would like to express my appreciation to the AFM guys, Jordi and Jerard and also to the crystallographers.

I would also like to acknowledge my Mom, Dad and my little Sister, who always being my wings, helped with my dreams and were really patient during these crazy times. Without their love, support and encouragement it would not have been possible to conquer my dreams.

I also have to be thankful to my Biochemist Mentor, an incredible and passionate man, a great person and Professor (also the "craziest" one), Dr. Aureliano Alves. He is responsible for all my enthusiasm in science and all my curiosity, he taught me to question everything, to work hard and do my best.

Another person who always was there for me was Dr. Lídia Dionisio, a great woman and a devoted teacher, who gives everything to her students.

Last but not least I want to thank to my Patricia and Eric, two of the most important persons in my life, who helped me no matter what, with love, support and encouragement in every step of my journey.

Resumo

Copper compounds (Schiff bases) as DNA-Interacting Agents

O cobre e o zinco são elementos ubíquos apresentando um papel essencial nos sistemas biológicos. Estas características, aliadas à sua química redox extremamente rica torna-os excelentes aliados no desenho de novos complexos com actividades anti-tumorais [1].

Os conhecimentos adquiridos sobre a estrutura química e processos bioquímicos envolvidos na formação e desenvolvimento de tumores permite-nos conceber novas estratégias para a sua prevenção e tratamento.

São conhecidos vários tipos de interacção dos compostos com o ADN, sendo uma das mais estudada a oxidação do ADN através da geração de espécies radicalares de oxigénio (ROS) [2].

À alguns anos foi sintetizado um complexo mononuclear de cobre(II), [CuII(pyrimol)-Cl] (onde pyrimol significa 4-metil-2-N-(2-piridilmetilen)aminofenolato). Este complexo revelou propriedades de clivagem do ADN extremamente promissoras [3].

Verificou-se também que os produtos de coordenação deste ligando com cloreto de zinco (II) ou acetato de zinco (II) também apresentava uma capacidade oxidativa de corte do ADN [4].

De acordo com as propriedades únicas evidenciadas por este ligando, foram desenhados novas bases de schiff baseadas no mesmo, tendo sido preparados os seus respectivos produtos de coordenação quer com cobre (II) quer com zinco (II).

As propriedades de interacção com o ADN foram estudadas com o auxílio de várias técnicas, tais como electroforese em gel de agarose, microscopia de forças atómicas, ensaios competitivos de fluorescência e ensaios de viscosidade.

Palavras-chave:
Cobre, Zinco, Bases de Schiff, Interacções com o ADN e clivagem do ADN.

Abstract

Copper compounds (Schiff bases) as DNA-Interacting Agents

Copper and zinc are ubiquitous compounds and they play an important role on biological systems. These characteristics, allied with the rich redox-active metal chemistry can be useful tools to design new complexes that can act as anticancer drugs [1].

We have different ways to damage DNA. The cleavage of the DNA strands can be achieved through the oxidation of the sugar moieties by the generation of reactive oxygen species (ROS) [2].

A few years ago, a simple mononuclear copper(II) complex, namely [CuII(pyrimol)-Cl] (where pyrimol stands for 4-methyl-2-N-(2-pyridylmethylene)aminophenolato was prepared, which showed unique DNA-cleaving properties [3]. In addition, the reaction of zinc(II) chloride or zinc(II) acetate with the ligand Hpyrimol has led to coordination compounds that are capable of cleaving DNA in an oxidative manner [4].

Considering this unique behavior of Hpyrimol, new Schiff-base ligands inspired by Hpyrimol have been designed, and coordination compounds with copper(II) and zinc(II) have been prepared. The potential DNA-Cleaving and interacting properties of these complexes has been investigated using gel electrophoresis, Atomic-Force Microscopy (AFM), ethidium bromide fluorescence competition binding assays and viscosimetry measurements.

Key Words
Copper, Zinc, Schiff-base, DNA Interactions and Cleavage

Table of contents

List of Figures

List of Tables

Abreviation List

ACN	acetonitrile
AFM	atomic force microscopy
Calf thymus DNA	CT-DNA
EA	Elemental analysis
EDTA	Ethylenediaminetetraacetic acid
ESI-mass	electrospray ionization mass spectrometry
EtBr	ethidium bromide
HEPES	2-(4-(2-Hydroxyethyl)- 1-piperazinyl)-ethansulfonic acid
^{1}H-NMR	proton nuclear magnetic resonance spectroscopy
IR	infrared spectroscopy
mmol	Micromole
ml	Mililiter
M	Molar (mol dm^{-3})
RT	room temperature
TBE Buffer	45 mM Tris base, 45 mM boric acid and 1 mM EDTA
EDTA	Ethylenediaminetetraacetic acid
Tris	tris(hydroxymethyl)aminomethane

Chapter I: Introduction

In the past decade the boundaries between biology and chemistry are becoming very thin, multidisciplinary has become an important and challenging tool to develop and enhance the proprieties of numerous drugs.

Cancer is a widespread disease and according to the World Health Organization caused 7.9 million deaths (around 13% of all deaths) in 2007, and we can estimate that with its continuing and rapid rise, there will be approximately 12 million deaths in 2030. The most affected areas are the lungs, stomach, liver, colon and breast, although, about 30% of cancer deaths can be prevented by the combinations of different therapies with synergistic interactions [5].

Biologic aspects of cancer

The usual definition of cancer is a group of malignant neoplastic disorder without a specific origin focus, involving dynamic alteration in the genome. In detail, we can describe it as an abnormal growth of cells, quick and uncontrolled leading to proliferation. This mass has a lack of differentiation and consequently the ability to invade adjacent tissues and undergo in a metastasis process by the invasion of the lymphatic system or the bloodstream [6-8].

Cancer can either have genetic or environmental causes, and in most cases there is a synergistic cooperation between these factors. Environmental causes can be characterized by the stepwise accumulation of successive mutations caused by biologic (virus), chemical (genotoxic and epigenetic agents) and physical (radiation) agents. These carcinogenic agents can alter some proto-oncogenes, activating or inactivating them, this process is known as initiation. The other stage is the promotion, known by the accumulation of mutations (due to a malfunction of the repairing systems). The last step in this cycle is the progression, process that can lead to the proliferation of the partial altered cell, becoming a highly malignant derivate.

The complex process of angiogenesis is essential for the growth, invasion, and metastasis of tumor cells. Understanding the chemical and biochemical pathways of this multistep process can help us find more efficient compounds to diagnose and treat cancer [9].

Cancer cells present defects in regulatory pathways that can lead to a defective mechanism of cell proliferation and homeostasis. According to this, current cancer treatments are multimodal, can involve integrated and complementary surgical techniques and therapies and sometimes the conjunction of chemotherapy with radiotherapy, or one of the above. In the clinical routine we can find antimetabolites that interfere with DNA synthesis and therefore cell division (like folic acid antagonists such as methotrexate), DNA-complexation agents, mitosis inhibitors, hormones and chemical reactive compounds such as alkylating agents (that cause direct DNA damage, such as nitrogen mustard and its derivatives, exemplified in Figure 1) and intercalating agents (such as actinomycins, that can inhibit the activity of a serious number of enzymes) [8, 10, 11].

Rosa Maria Faustino Brissos – DQB – FCUL

Nowadays treatments have enormous undesired side effects, due to the nonspecific toxicity. Therefore cancer research is focused on the design of new drugs with greater sensibility and specificity with the minimal drug resistance [6, 12].
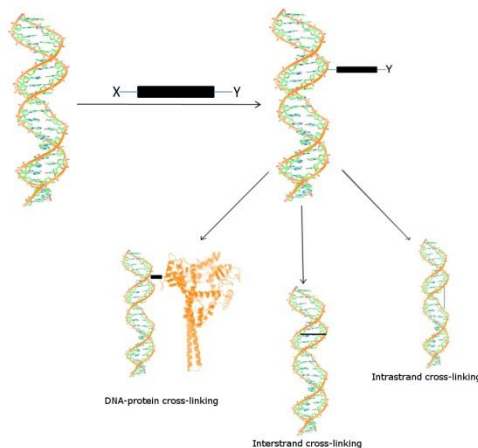
Figure 1: Example of alkylation and the different modes of DNA cross-linking [6].

Bioinorganic chemistry

Bioinorganic chemistry is a recent discipline in the inorganic field, despite reports that talk about the incorporation of metal in enzymes that date back to the 19th century and even earlier. The interdisciplinary approach between coordination chemists, chemical physicists, and biochemists lead to the creation of this extraordinary and prominent discipline [13].

Inorganic compounds have been used in medicine for centuries because they fulfill important roles in biological processes. Being applied either in therapeutics or as diagnostic aids [13-16].

Metals are essential cellular components, playing an important role in biochemical processes for living organisms. The bioavailability of these elements, the rich redox proprieties, the variable coordination modes and reactivity were key factors to their bioincorporation in the biological systems, namely in one third of all known enzymes. Therefore, drugs based in transition metal compounds can be synthetized and applied in a wide range including anticancer agents, anti-infective, and immunosuppressive, and are used on the treatment of rheumatoid arthritis, and metabolic disorders [9, 17, 18].

Cancer chemotherapy is a very complex investigation field, nevertheless it is experiencing a quiet rapid growth. The first discoveries in the field were based on the observations of some poisoning gases, as nitrogen mustard, with some therapeutic effects during World Wars I and II by Goodman and his co-workers [19]. Later on, therapies using folate and purine analogs also showed some DNA interactions, as well as some alkaloids (used as anti-diabetic drugs) were identified as tumor cell division blockers. Nowadays, some of these therapies remain in clinical use, in synergy, concept integrated in the 1960s [20].

Another important mark in chemotherapy research was the accidental discovery of a remarkable inorganic antitumor compound, cisplatin. This compound is the most used compound in chemotherapeutic agents [9, 14].

Metal based compounds have numerous advantages when compared to the organic ones. The ability to coordinate with several different ligands can be a useful tool to functionalize the compound. The alteration of the kinetic and redox proprieties as well as the three dimensional structure can improve the specificity, the efficiency and, in an ideal situation, decrease the toxicity of the compound. The interaction with the balanced cell redox state, by activating an inert compound can tune the inherent toxicity of the drug, so we can target cancer cells [9, 10].

The biological role of copper and zinc

Copper and Zinc enzymes have a long history of cooperation in evolutionary biology. The necessity in multicellular systems brought together two important classes of metalloproteins in order to enhance a dynamic homeostasis. One of the most important characteristics that makes the difference in the study and development of possible antitumoral agents based in inorganic compounds is the fact that copper and zinc are essential trace elements and they play an important and decisive role in biology. Anticancer compounds based on them are, hypothetically, less toxic and more effective [21, 22].

Copper

Copper is an important trace element, and we can find it in almost all organisms, essentially in enzymes and proteins, and plays a crucial role in biological redox chemistry involving molecular oxygen to produce free radicals, in growth and in development [21, 23].

Alterations on copper homeostasis can result in diseases such as Mankes and Wilson disorders but can also cause rheumatoid arthritis, gastrointestinal ulcers, epilepsy, diabetes and cancer. Copper toxicity is caused, essentially, by the ability of this metal to produce reactive oxygen species (ROS) that cause the lipid peroxidation and can directly cleave DNA and RNA [23].

In enzymes copper is present in mononuclear or coupled multinuclear configurations, evolutionarily configured to facilitate the redox process in the biological systems. It can also alter its oxidation state between Cu(I), Cu(II) and Cu(III). In Figure 2 we can see an example of Cu- containing enzymes, and most are O_2 activated function enzymes such as dioxygenases, monooxygenases, and oxidases [24].

The explanation for the toxicity of copper is the alteration of the cellular redox balance. The generation of ROS (Fenton chemistry) by cupric and cuprous ions in the presence of superoxide or by reducing agents such as ascorbic acid or glutathione (GSH) leads to the redox-signaling pathways. The cellular environment alteration triggers a cascade of reactions, named apoptotic pathways which finally lead to apoptosis [23, 25].

In literature we found evidences that copper binding compounds have selectivity to tumor cells, inducing apoptosis by the accumulation of ubiquinated proteins comparatively to "normal" cells [23]. This selectivity is due to the selective permeability of cellular membranes to copper compounds [26].

Bioinorganic chemists have been appealed to design new complexes in order to exploit all the potentialities of the oxidative nature of this essential element. Since the

Rosa Maria Faustino Brissos – DQB – FCUL

discovery and characterization of the chemical nuclease propriety of $[Cu(phen)_2]^{2+}$ (phen = 1,10 Phenantroline), due to the strong interaction with DNA, new heterocyclic complexes have been synthetized [25, 27]. Cu(II) centered compounds are reported to be promising and/or are being used as a viable alternative to Cisplatin, one of the most worldwide used anticancer drug [22, 28]. The nuclease activity, *in vivo* and *in vitro*, of these complexes have been documented not only as cytotoxic agents but also by the ability to trigger cellular apoptosis *in vitro* [2, 29-31].
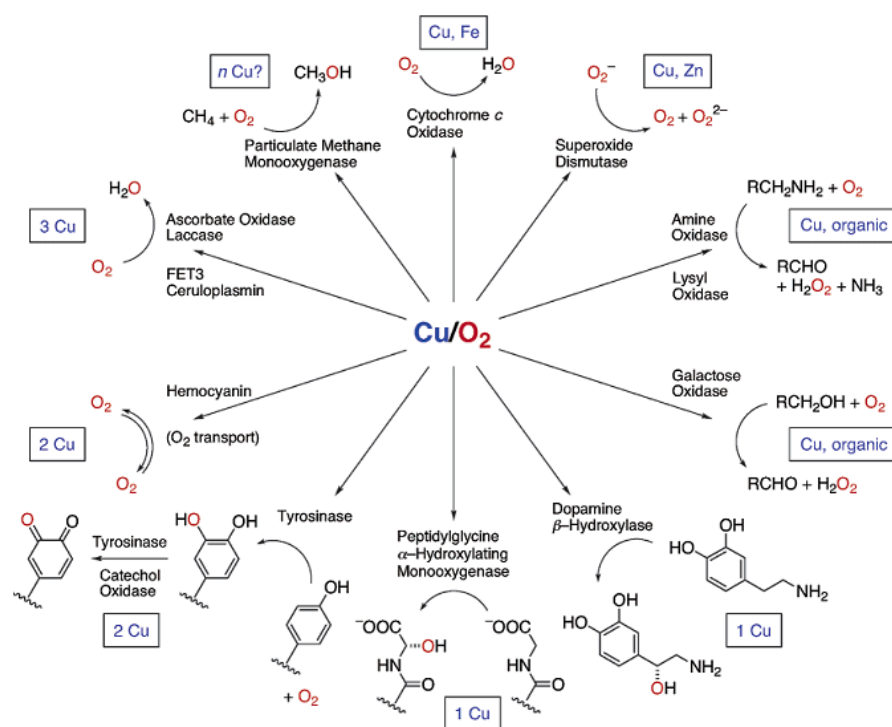
Figure 2: Example of the biological relevance of Cu in biochemical processes. In the figure we can see different enzymes and proteins that Cu activates. Adapted from [24].

Schiff bases represent an important class of compounds in medicinal chemistry by themselves [32]. They have been considered privileged ligands, because they have an easy synthesis by being prepared from condensation of aldehydes or ketones with amines. They are extremely versatile, their chemistry is flexible, selective and sensible to a wide number of metal ions. Other positive remark of these ligands is the fact that they can stabilize various oxidation numbers. They can be used in a wide range of applications since organic degradation, corrosion inhibitors to drug development. When conjugated with metals they have unique properties such as photoluminescence and electroluminescence [32-34]. It is described that Schiff bases coordinated to Cu(II) have antiproliferative and antibacterial activities, due to the properties of the ligands allied to the structural and electronic properties of metal coordination [25].

Since 1960, thiosemicarbazones, imidazoles and phosphines awakened the interest of scientists due to potential medical interest, in detail as anticancer agents. The respective copper complexes, followed by p-acceptor-type ligands complexes are a class of compounds with growing medicinal interest, because they exhibit antibacterial,

4

antiviral, antiparasitic, anticancer, and antifungal activity. Some of the Cu-thiosemicarbazones, used in clinical practice as antiviral, are for example methisazone or marboran (N-methyl-isatin-8-thiosemicarbazone) and 3-AP or triapine (3-aminopyridine-2-carboxaldehyde-thiosemicarbazone) [35].

Zinc

Zinc is one of the most available trace elements, consequently is not surprising the fact that biology took advantage of its great capabilities. It is the second transition metal most abundant in the human body and presents a Lewis acid character, one of the reasons for its critical role in cell proliferation, differentiation and defense against free radicals. It is a structural element in proteins and enzymes including transcription and growth factors, cellular signaling proteins, neurotransmission and DNA repair enzymes. There are known approximately 300 zinc enzymes from different classes, oxidoreductases, transferases, hydrolases, lyases, isomerases, and ligases (Figure 3B). Prokaryotic and eukaryotic cells have some differences in their zinc metabolism [9, 21, 36, 37].

Alterations in the biological levels of zinc can result in systemic abnormalities, including growth retardation, immunodeficiency, hypogonadism, neuronal and sensory dysfunctions and the development of cancer. Zinc homeostasis is carried out through Zn transporters, permeable channels and metallothioneins (Figure 3A). [38].
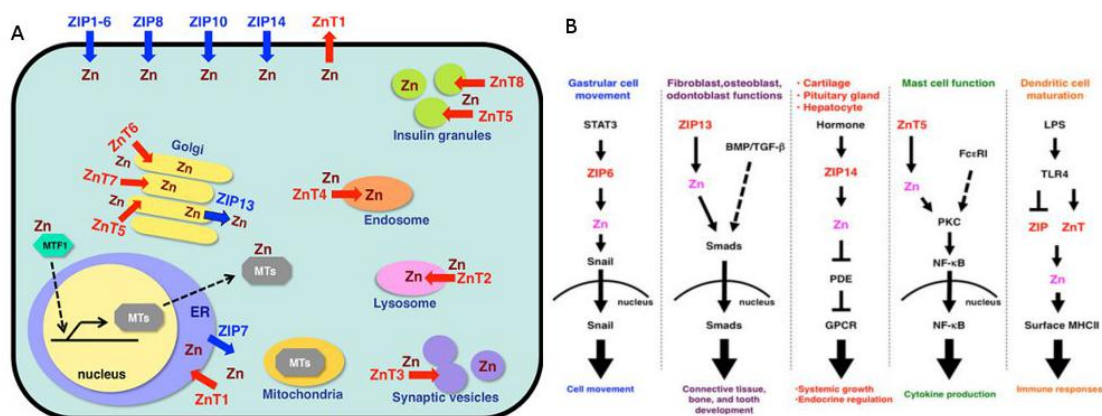
Figure 3: Zinc localization in the cell, transporters and Methalothionines (A) and its main functions in biologic systems (B). Adapted from [38].

Its therapeutic and preventative effects have also been reported on infectious diseases such as malaria and pneumonia [36]. Some zinc complexes also have revealed to be anti-tumoral because many of its compounds are known to act as synthetic hydrolases towards the phosphodiester cleavage of the DNA. Recently, it has been reported that, against all expectations some square planar zinc (and copper) complexes can act as nucleases, Hpyrimol and Hpyramol, cleaving oxidatively DNA [39].

Zinc complexes can present fluorescence properties that can be used for imaging, as sensors. These probes can be useful tools in the study of biochemical pathways or in the study of intake of some drugs and its cellular pathway [14, 40].

5

DNA cleavage

In cancer therapy, DNA is a target molecule and has become an interesting foundation for the development of biologically active agents. Actually, DNA is treated as a non-specific target of the cytotoxic agents. The efficiency of the treatment was improved with the use of these alkylating agents, unfortunately they are extremely toxic. The main goal of cancer research is to increase the efficiency of the drugs by decreasing their toxicity [41, 42].

DNA is one of the major and most attractive research targets in discovery and development of chemical drugs. The molecular interactions of metal ions with DNA can either be by diffuse binding or site binding. In the first binding mode the interaction is carried out by the water molecules with long range Coulombic interactions allowed by the accumulations of the positive metal ions around the nucleic acid. In the site binding mode, the metal ions can be coordinated to specific binding sites, by the inner-sphere of coordination (direct mode) or the outer sphere of coordination (indirect mode, through a water molecule). The different metal ions have different nucleic acid monomeres, being the guanine N7 (preferred by Cu(II) complexes for covalent bounding), adenine N1 and/or N7, cytosine N3, thymine O4 and/or N3 (recognized by Zn(II) complexes) the "preferred" sites at physiological pH for the 3d transition metal ion - nucleobase complexes [26].
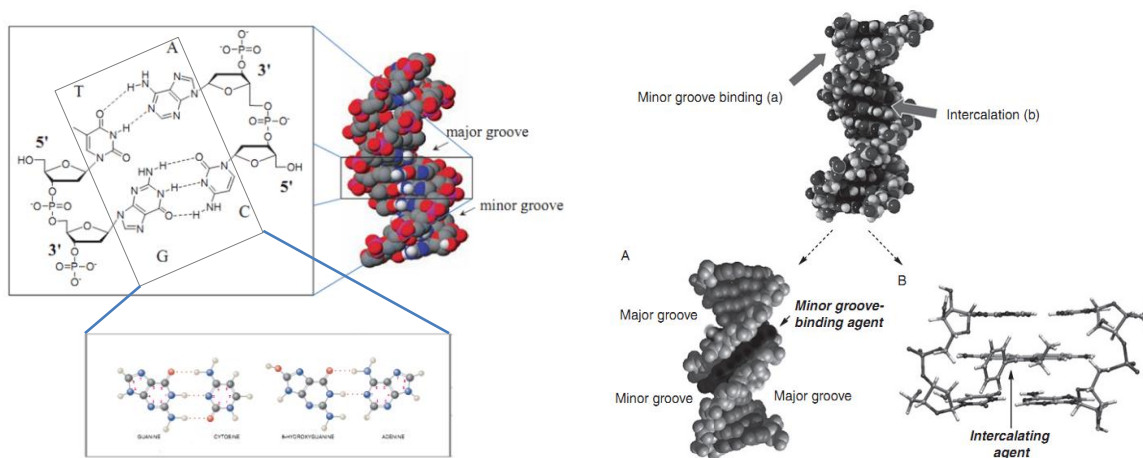
Figure 4: Molecular representation of DNA with complimentary pairs of nucleotides. (Adapted from [43, 44]) .

As we said before, the interactions of the drug with DNA can be either irreversibly covalent or reversibly non-covalent bindings. The covalent interactions can be essentially by sugar-phosphate backbone binding, the intercalation between the base pairs, alkylations, cross linking of strands, covalent binding or metal-coordination The non-covalent interactions can be further classified by the intercalation of the major or the minor groove (Figure 4). These interactions are possible due to DNA's large number of donor sites for binding, the H- bonding donor/ acceptor sites and finally the important potential π-π stacking [42, 43, 45].

Rosa Maria Faustino Brissos – DQB – FCUL

Intercalations, covalent binding or groove binding, have an indirect DNA damage because they don't alter the DNA *per se* but they alter the activity of the enzymes responsible for maintaining the integrity of DNA. These interactions happen with the formation of strong hydrogen bonds, damaging the DNA through several DNA binding modes (depending on the compound) [11]. Nowadays many scientists are focused on the design of metallonucleases based on copper and zinc centers, and the analytical, computational and molecular biology developments become essential to understand in detail molecular insight into the cleavage mechanism. Many transitions metals present oxidative behavior in the presence of oxidants or reductants. This behavior is demonstrated by the attack to the sugar moiety of DNA (a proposal and schematic example is presented on the Figure 5) [46].
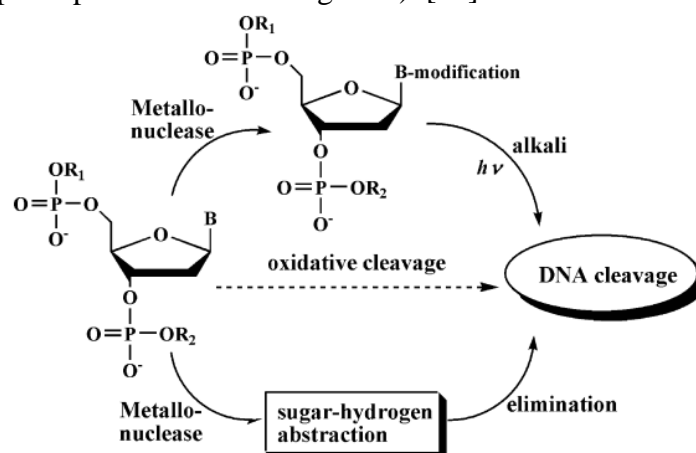
Figure 5: DNA strand scission induced by nucleobase modification or sugar-hydrogen abstraction (modified based on Refs. [46-48]

The oxidative DNA mechanism can be caused by reactive oxygen or metal-oxo species, nucleobase modification or hydrogen abstraction of sugar moiety including single electron transfer, hydrogen atom transfer or proton-coupled electron-transfer processes. Transition metals have an important role in the redox cycle in order to form primary and secondary ROS and RMOS. The generation of ROS (schematic presented on Figure 6) , by typical Fenton-type reaction, produces hydroxyl radical ($\cdot OH$), hydrogen peroxide (H_2O_2), and the superoxide anion (O_2^-), and they can promote DNA damage, adding double bonds of DNA bases or abstracting hydrogen atoms from sugar moiety[46].
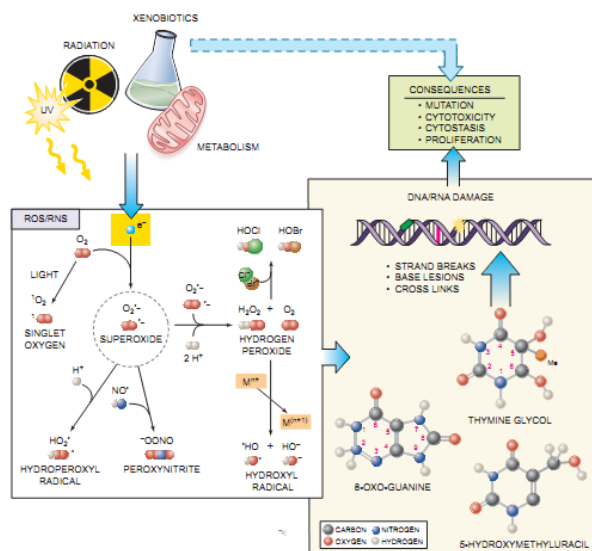
Figure 6: Exogenous and endogen processes of reactive oxygen species (ROS) and reactive nitrogen species (RNS) and his consequent actions. Adapted from [44].

In Figure 7 we can schematically see the mechanism of these DNA damage. The sugar scission at the sugar moiety depends on the reactivity of the seven hydrogen atoms, the Hydrogen atoms at C1, C4 and C5 are accessible from minor grooves while those placed on the C2 and C3 are accessible from major grooves. Most of metallonucleases are designed to bind to the minor groove because of the lower accessibility of the major groove, and also the lower reactivity [46, 47].
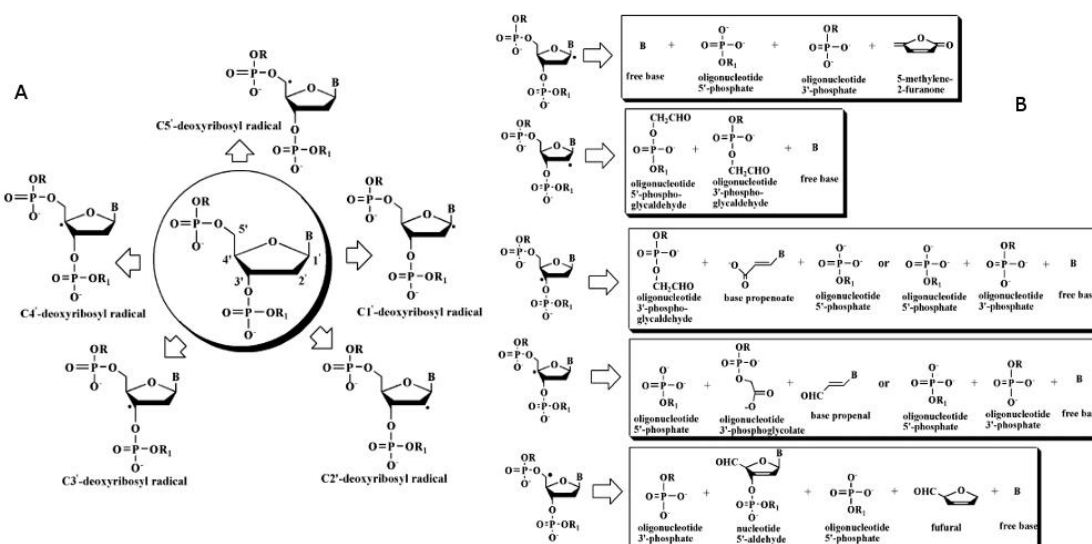
Figure 7: Products originated by the hydrogen abstraction, deoxyribosyl radicals (A) and scission products from this abstraction (adapted from[46])

New drugs face many associated and limiting problems, as the nonspecific toxicity related to the biodistribution of the drugs, pharmacokinetics and pharmacodynamics' behavior. Besides, the mechanistic details of cellular uptake of the clinical recurrent chemotherapeutics are extremely incomplete [6, 11, 14].

8

Rosa Maria Faustino Brissos – DQB – FCUL

Another critic problem on cancer chemotherapy is resistance. Cells have complex mechanisms and they can develop resistance to drugs. The resistance is due to the decrease in membrane transport, the increase of the drug detoxification and the increase of DNA repair and tolerance to DNA damage [43].

The essential targets of the chemotherapy agents are the pathways of cellular division, being cytostatic or cytotoxic.

Rosa Maria Faustino Brissos – DQB – FCUL

Chapter II: Objectives

This work aims to synthesize, characterize and study the DNA interactions of a new series of Zn(II) and Cu(II) complexes. The coordination reactions of these family of ligands will be carried out with different transition-metal salts $CuCl_2 \cdot 2H_2O$, $ZnCl_2$.

The first part of this work consisted in the synthesis of a series of ligands, (E)-2-((quinolin-2-ylmethylene)amino)phenol, (E)-4-methyl-2-((quinolin-2-ylmethylene)amino) phenol, (E)-4-(tert-butyl)-2-((pyridin-2-ylmethylene)amino)phenol, (E)-2-(((2-hydroxyphenyl)imino)methyl)pyridine 1-oxide, (E)-2-(((2-hydroxy-5-methylphenyl)imino)methyl)pyridine 1-oxide,. After the characterization with the usual techniques, the complexes with Cu(II) and Zn(II) where prepared and then they were also characterized with ESI-mass, Elemental analysis (EA) and IR spectroscopy.

The second part of this work aimed to determine the DNA interaction behavior of the different complexes. In this part, the binding studies and the cleavage ability were evaluated using pBR322 DNA and calf thymus by different techniques such as electrophoresis, atomic force microscopy, viscosity and fluorescence assays.

These complementary techniques allow us to infer the interactions between the complexes and DNA. The intercalation mechanism can be investigated using fluorescence or viscosity. Fluorescence using ethidium bromide (EtBr) is a simple and useful technique that helps us to verify the EtBr displacement by the studied compounds through the observation of a decreasing on the fluorescence intensity. Other helpful technique is the viscosity, it give us information on interaction behavior of the complexes.

The DNA-interacting and nuclease potential behaviors can be observed by AFM (atomic force microscopy) and electrophoresis. AFM allows the observation of structural transitions in the tertiary structure of plasmidic DNA by the appearance of kinks and compactions. Electrophoresis as well, gives us qualitative information (and with the perfect conditions we also obtain some quantitative information). We can study the appearance of DNA form II (nicked) and form III (linear) when DNA is incubated with different concentrations of the complexes.

Chapter III: Experimental Section

3.1. Reagents and Material

All reagents and solvents were used as received from Sigma or Aldrich.

IR spectra were recorded in solid state (KBr pellets) on a NICOLET 5700 FT-IR spectrometer at the Inorganic Chemistry Department of the University of Barcelona.

The Elementary Analyses (EA) for the elements C, H, N and S were performed on a Carlo Erba EA1108 analyzer at the Serveis Cientifico-Tecnics of the University of Barcelona.

Mass Spectrometry was carried out both using a Maldi-TOF VOYAGER DE-RP mass spectrometer with a nitrogen laser (337 nm, 3 ns pulse) and the accelerating voltage of 20-25 kV and a LC/MSD-TOF ESI-mass spectrometer from AGILENT TECHNOLOGIES at the Serveis Cientifico-Tecnics of the University of Barcelona.

^{1}H-NMR spectra were recorded at RT on a VARIAN UNITY (300 MHz) at the Serveis Cientifico-Tecnics of the University of Barcelona. All samples were dissolved in CDCl$_3$ and the proton chemical shifts were referenced to δ(CDCl$_3$) = 7.26 ppm.

The biological assays were perfomed with 10 mM Tris-HCl, 0,1mM EDTA 50 mM NaCl and 40 Mm HEPES, 10 mM MgCl$_2$.

AFM images were obtained by a NANOSCOPE III MULTIMODE AFM microscope from DIGITAL INSTRUMENTS Inc. at the Serveis Cientifico-Tecnics of the University of Barcelona. It was operated with a Nano-crystalline Si cantilever of 125 nm length and a spring constant of 50 N/m. The conical-shaped Si probe tip contained a 10 nm apical radius and 35° cone angle.

Agarose gel electrophoresis was performed in the horizontal bucket ECOGEN, connected to the voltage source of a PHARMACIA GPS 200/400. The gels were photographed using a FUJIFILM FTI-500 camera.

Fluorescence measurements were performed on a HORIBA Nanolog iHR 320 spectrophotometer in the Inorganic Department of the University of Barcelona.

Viscosity measurements were performed on Vibro Viscosímeter SV-1ª de *AND A&N Company Limited* in the Inorganic Department of the University of Barcelona.

3.2. Synthesis and characterization

3.2.1. Ligands

3.2.1.1 Synthesis of (E)-2-((quinolin-2-ylmethylene)amino)phenol - L1

Adapted from the literature [39]. A solution of 2-quinolinecarboxaldehyde (1.96 g, 0.1 mol) in methanol (9.4 mL) was added, under constant stirring, to a solution of 2-aminophenol (1.4 g, 0.1 mol) in methanol (0.625 mL). The reaction mixture was heated at reflux (70 ºC) for 2 h. The mixture starts to precipitate to yield a yellow solid. This solid material was collected and washed with
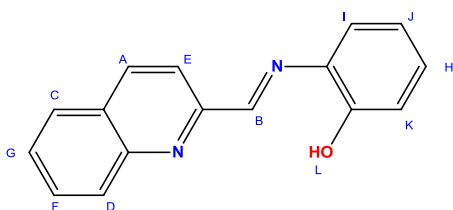
diethyl ether, and was subsequently dried a vacuum chamber. Yield: 62%.

$C_{16}H_{12}N_2O$; Molecular Weight: 248.28;

1H-NMR (CDCl₃, 300 MHz) δ 9.01 (s, 1H, A), 8.31 (dd, 1H, B), 8.25 (dd, 1H, C), 8.17 (dd, 1H, D), 7.88 (dd, 1H, E), 7.79 (m, 1H, F), 7.62 (m, 1H, G), 7.47 (dd, 1H, H), 7.27 (m, 1H, I), 7.07 (dd, 1H, J), 6.96 (m, 1H, K) ppm;

IR (neat) 3428, 3039, 2822, 2672, 2540, 1598, 1503, 1452, 1373, 1289, 1106, 937, 887, 831, 773, 749, 632, 482cm⁻¹.

Elemental analysis: N, 4.64± 0.25; C, 76.97 ± 0.15; H, 11.27 ± 0.11

MS (ESI): m/z 248.9 (M + H), 246.9, 250.0, 251.0

3.2.1.2 Synthesis of (E)-4-methyl-2-((quinolin-2-ylmethylene)amino) phenol - L2

Adapted from the literature [39]. A solution of 2-quinolinecarboxaldehyde (1.96 g, 0.1 mol) in methanol (9.4 mL) was added, under constant stirring, to a solution of 2-amino-4-methylphenol (1.5 g, 0.1 mol) in methanol (0.625 mL). The reaction mixture was heated at reflux (70 ºC) for 2 h. The mixture starts to precipitate to yield a yellow solid. This solid material was collected and washed with diethyl ether, and was subsequently dried in a vacuum chamber. Yield: 43%;
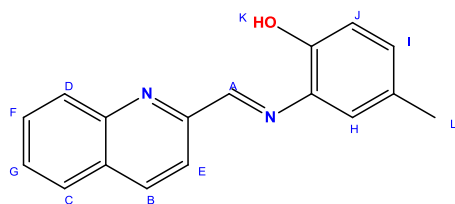
$C_{17}H_{14}N_2O$; Molecular Weight: 262,31

1H-NMR (CDCl₃, 300 MHz) δ 8.98 (s, 1H, A), 8.30 (dd, 1H, B), 8.24 (dd, 1H, C), 8.16 (dd, 1H, D), 7.87 (dd, 1H, E), 7.77 (m, 1H, F), 7.61 (m, 1H, G), 7.28 (dd, 1H, H), 7.07 (dd, 1H, I), 6.95 (dd, 1H, J), 6.96 (m, 1H, K), 2.33 (m, 1H, L) ppm;

IR (neat) 3019, 2915, 1597, 1564, 1502, 1427, 1365, 1287, 1248, 1206, 1188, 1122, 837, 785, 755, 580, 481 cm⁻¹.

Elemental analysis: N, 10.79 ± 0.51; C, 78.41 ± 2.69; H, 5.233 ± 0.092

MS (ESI): m/z 263.0 (M + H), 264.1, 265.1, 261.1.

3.2.1.3 Synthesis of (E)-4-(tert-butyl)-2-((quinolin-2-ylmethylene)amino) phenol – L3

A solution of 2-quinolinecarboxaldehyde (1.07 g, 0.1 mol) in methanol (10 mL) was added, under constant stirring, to a solution of 2-amino-4-tercbutilphenol (1.7 g, 0.1 mol) in methanol (7.5 mL). The reaction mixture (orange) was heated at reflux (70 ºC) for 2 h. After this time, the green solution was evaporated under reduced pressure. This oil was solved in diethyl ether (10 mL) and precipitated with 20 mL of benzene. The mixture starts to precipitate to yield a green solid. This solid material was collected and washed with n-hexane, and was subsequently dried in a vacuum chamber. Yield: 72%;
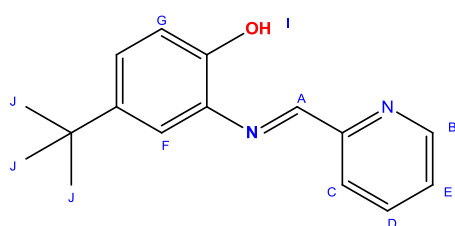
$C_{16}H_{18}N_2O$; Molecular Weight: 254,33

1H-NMR (CDCl₃, 300 MHz) δ 8. 87 (s, 1H, A), 8.73 (m, 1H, B), 8.24 (d, 1H, C), 7.83 (m, 1H, D), 7.43 (dd, 1H, E), 7.39 (m, 1H, F), 7.30 (dd, 1H, G), 7.07 (s, 1H, H), 6.97 (d, 1H, I), 1.20 (m, H, J)ppm;

IR (neat) 3078, 2959, 2900, 2865, 2360, 1587, 1569, 1503, 1472, 1438, 1361, 1290, 1213, 1167, 821, 801, 769, 743, 512 cm^{-1}.

Elemental analysis: N, 10.98±0.014; C, 74.86±0.035; H, 7.63±0.035

MS (ESI): m/z 255.14 (M + H), 277 (M + Na)

3.2.1.4 Synthesis 2-Pyridinecarbaldehyde N-oxide
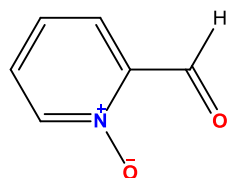
Adapted from the literature [49]. A mixture of picoline N-oxide (5.45g, 50 mmol) and selenium dioxide (5.54 g, 50 mmol) in pyridine (25 ml) was heated under reflux for 5 h. The solid material was filtered off, the filtrate was concentrated in vacuum, and the residual oil was extracted four times with hot toluene (50 ml). The yellow liquid was concentrated on vacuum. If the residual oil is pure it will solidify. This solid material (yellow) was collected and washed with diethyl ether, and was subsequently dried in a vacuum chamber. Yield: 18%;

$C_6H_5NO_2$ Molecular Weight: 123.11

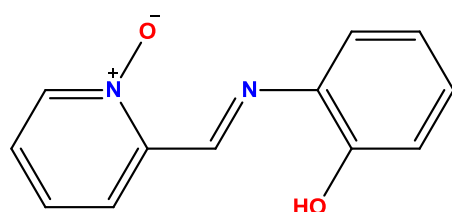^{1}**H-NMR** (CDCl$_3$, 300 MHz) δ 10.64 (s, 1H, A), 8.22 (d,1H, B), 7.83 (dd, 1H, C), 7.47 (m, 1H, D), 7.33 (m, 1H, E), 7.27 (s, 1H, F), ppm;

IR (neat) 3265, 3082, 2698, 1692, 1656, 1617, 1470, 1441, 1345, 1280, 1237, 1202, 1057, 1015, 851, 764, 735, 648, 570, 526 cm^{-1}.

Elemental analysis: N, 11.42, C, 58.25; H, 4.09

MS (ESI): m/z 123.8 (M + H), 140.9 (M+NH$_4$).

3.2.1.5 Synthesis of (E)-2-(((2-hydroxyphenyl)imino)methyl)pyridine 1-oxide –L4

A solution of 2-Pyridinecarbaldehyde N-oxide (0.47 g, 0.1 mol) in methanol (5 mL) was added, under constant stirring, to a solution of 2-aminophenol (0.42 g, 0.1 mol) in methanol (5 mL). The reaction mixture was heated at reflux (60 ºC) for 20 min. The mixture starts to precipitate to yield a yellow solid. This solid material was collected and washed with n-hexane, and was subsequently dried in a vacuum chamber. Yield: 64%;
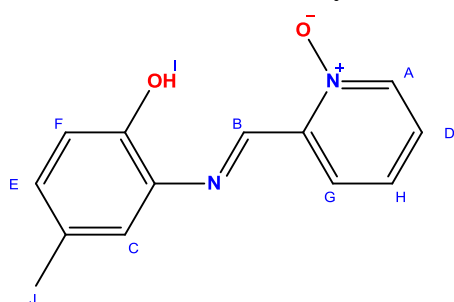
$C_{12}H_{10}N_2O_2$ Molecular Weight: 214.22

IR (neat) 3344, 3119, 3040, 2359, 1917, 1791, 1699, 1589, 1492, 1491, 1431, 1292, 1255, 1186, 1159, 1139, 1088, 867, 754, 678, 516, 490 cm^{-1}.

Elemental analysis: N, 13.12±0.042, C, 66.93±0.057; H, 4.345±0.092

MS (ESI): m/z 215,08 (M + H)

3.2.1.6 Synthesis of E)-2-(((2-hydroxy-5-methylphenyl)imino)methyl)pyridine 1-oxide –L5

A solution of 2-Pyridinecarbaldehyde N-oxide (0.80 g, 0.1 mol) in methanol (5 mL) was added, under constant stirring, to a solution of 2-amino-4-methylphenol (0.82 g, 0.1 mol) in methanol (mL). The reaction mixture was heated at reflux (60 ºC) for 20. The mixture starts to precipitate to yield a yellow solid. This solid material was collected and washed with diethyl ether, and was subsequently dried in a vacuum chamber. Yield: 43%;

$C_{13}H_{12}N_2O_2$, Molecular Weight: 228.25

^{1}H-NMR (CDCl$_3$, 300 MHz) δ 9.46 (s, 1H, A), 8.26 (dd,1H, B), 8.16 (dd, 1H, C), 7.34 (m, 1H, D), 7.30 (, 1H, E), 7.26 (s, 1H, F), 7. 08 (dd, 1H, G), 6.92 (d, 1H, H), 1.58 (s, 1H, J) ppm;
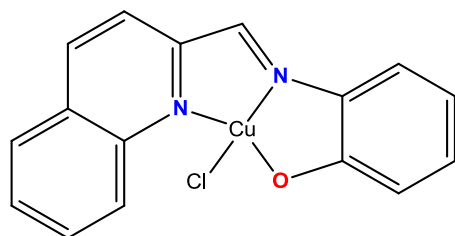
IR (neat) 3105, 3078, 3040, 3019, 2910, 2857, 1599, 1503, 1485, 1430, 1343, 1295, 1199, 1163, 1115, 836, 794, 760, 743, 529 cm^{-1}.

Elemental analysis: N, 12.10, C, 67.80, H, 5.15

MS (ESI): m/z 229,09 (M + H), 251 (M + Na)

3.2.2. Complexes

3.2.2.1 Synthesis of Complex 1

An emulsion of 50 mg (2.01×10^{-4} mol) of ligand L$_1$ and 10 ml methanol was slowly added to a solution of 34 mg (2.01×10^{-4} mol) CuCl$_2$·2H$_2$O in 10 ml methanol. The resulting dark red reaction mixture was left unperturbed at room temperature for crystallization (slow evaporation of the solvent). Within a few weeks complex **1** was obtained as a black crystalline powder, which was washed with diethyl ether. Yield: 49.7%.
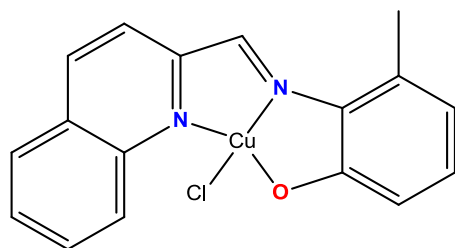
$C_{16}H_{11}ClCuN_2O$, Molecular Weight: 346.27.

IR (neat) 3416, 3058, 1369, 1587, 1548, 1513, 1462, 1376, 1344, 766 cm^{-1}.

Elemental analysis: N, 8.17±0.49, C, 52.59±0.22, H, 2,103±0,62

MS (ESI): m/z 337 (M - Cl), 311 (M - Cl)

3.2.2.2 Synthesis of Complex 2

An emulsion of 50 mg (1.91×10^{-4} mol) of ligand L$_2$ and 10 ml methanol was slowly added to a solution of 32 mg (1.91×10^{-4} mol) CuCl$_2$·2H$_2$O in 10 ml methanol. The resulting dark brown reaction mixture was left unperturbed at room temperature for crystallization (slow evaporation of the solvent). Within a few weeks complex **2** was obtained as a black crystalline

powder, which was washed with diethyl ether. Yield: 49.7%.

$C_{17}H_{13}ClCuN_2O$, Molecular Weight: 360.30,

m/z: 344.99 (100.0%), 346.98 (76.5%), 345.99 (17.5%), 348.98 (14.3%), 347.99 (13.4%), 349.98 (2.6%), 346.99 (1.7%), 348.99 (1.3%)
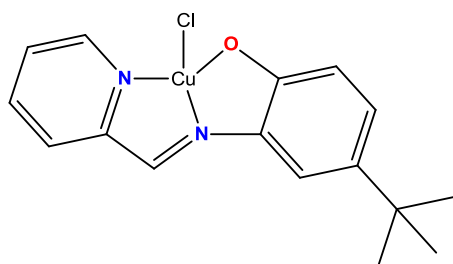
IR (neat) 3415, 3052, 2920, 2360, 2341, 1636, 1615, 1589, 1505, 1483, 1431, 1377, 1309, 1101, 804, 756 cm^{-1}.

Elemental analysis: N, 7.40±0.20, C, 56.48±0.25, H, 2.42±0.21

MS (ESI): m/z 323.03 (M - Cl), 325.02 (M - Cl), 324.03 (M - Cl) 311 (M - Cl)

3.2.2.3 Synthesis of Complex 3

An emulsion of 50 mg (1.97×10^{-4} mol) of ligand L$_3$ and 10 ml methanol was slowly added to a solution of 34 mg (1.97×10^{-4} mol) CuCl$_2$·2H$_2$O in 10 ml methanol. The resulting dark red reaction mixture was left unperturbed at room temperature for crystallization (slow evaporation of the solvent). Within a few weeks complex **3** was obtained as a black crystalline powder, which was washed with diethyl ether. Yield: 56%.

$C_{16}H_{17}ClCuN_2O$; Molecular Weight: 352.32;

m/z: 351.03 (100.0%), 353.03 (76.7%), 352.04 (17.5%), 355.03 (14.5%), 354.03 (13.8%), 356.03 (2.5%), 353.04 (1.7%), 355.04 (1.1%)
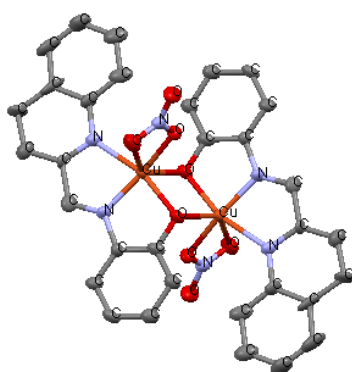
IR (neat) 3853, 3747, 3566, 3445, 2959, 2868, 2361, 2342, 1684, 1670, 1652, 1649, 1635, 1559, 1559, 1541, 1507, 1473, 1457, 1375, 1263, 827, 778, 668 cm^{-1}.

Elemental analysis: N, 7.21±0.047, C, 49.15±0.57, H, 4.42±0.28

MS (ESI): m/z 351.03 (M), 353.03 (M), 316.06, 318.06

3.2.2.4 Synthesis of Complex 4

An emulsion of 50 mg (2.01×10^{-4} mol) of ligand L$_1$ and 10 ml methanol was slowly added to a solution of 49 mg (2.01×10^{-4} mol) Cu(NO$_3$)$_2$·3H$_2$O in 10 ml methanol. The resulting dark red reaction mixture was left unperturbed at room temperature for crystallization (slow evaporation of the solvent). Within a few weeks complex **4** was obtained as a black crystalline powder, which was washed with diethyl ether. Yield: 67%.

$C_{32}H_{22}Cu_2N_6O_8$; Molecular Weight: 745.65;

m/z: 744.01 (100.0%), 746.01 (91.6%), 745.01 (37.1%), 747.01 (31.5%), 748.01 (27.3%), 749.01 (7.6%), 746.02 (6.0%), 747.00 (2.0%), 750.01 (1.7%), 747.02 (1.2%)
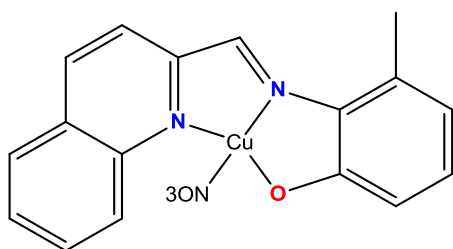
IR (neat) 3574, 3434, 1640, 1628, 1583, 1513, 1527, 1514, 1500, 1464, 1393, 1368, 1324, 1274, 1073, 769 cm^{-1}.

Elemental analysis: N, 7.24±0.10, C, 54.605±0.092, H, 2.97±0.064

MS (ESI): m/z 374 (M - H), 373.01 (M - H), 746.01 (2M), 747.01

3.2.2.5 Synthesis of Complex 5

An emulsion of 50 mg (1.91×10^{-4} mol) of ligand L_2 and 10 ml methanol was slowly added to a solution of 46 mg (1.91×10^{-4} mol) $Cu(NO_3)_2 \cdot 3H_2O$ in 10 ml methanol. The resulting dark red reaction mixture was left unperturbed at room temperature for crystallization (slow evaporation of the solvent). Within a few weeks complex **5** was obtained as a black crystalline powder, which was washed with diethyl ether. Yield: 43%.

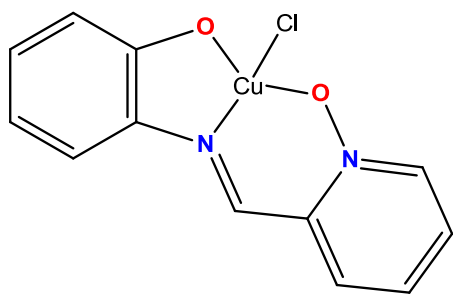$C_{17}H_{13}CuN_3O_4$, Molecular Weight: 386,85.

IR (neat) 3567, 3444, 2360, 2341, 1700, 1653, 1635, 1558, 1540, 1518, 1472, 1460, 1336, 1260, 1164, 1115, 945, 876, 814, 770, 668 cm^{-1}.

Elemental analysis: N, 8.61, C, 54.69, H, 3.33

MS (ESI): m/z 388.02 (M-H), 337 (M - Cl), 261.10 (M - CuCl)

3.2.2.6 Synthesis of Complex 6

An emulsion of 50 mg (2.33×10^{-4} mol) of ligand L_4 and 10 ml methanol was slowly added to a solution of 40 mg (2.33×10^{-4} mol) $CuCl_2 \cdot 2H_2O$ in 10 ml methanol. The resulting dark red reaction mixture was left unperturbed at room temperature for crystallization (slow evaporation of the solvent). Within a few weeks complex **6** was obtained as a black crystalline powder, which was washed with diethyl ether. Yield: 48%.

$C_{12}H_9ClCuN_2O_{22}$; Molecular Weight: 312.21.

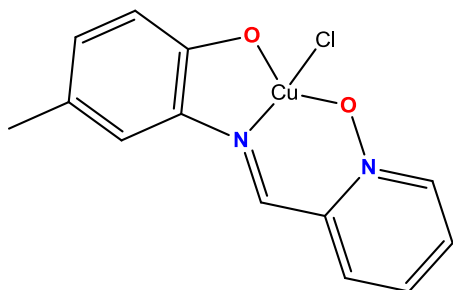Elemental Analysis: C, 46.16; H, 2.91; Cl, 11.36; Cu, 20.35; N, 8.97; O, 10.25;

IR (neat) 3435, 3065, 1585, 1484, 1470, 1430, 1387, 1279, 1254, 1397, 1153, 833, 768, 756, 627, 542 cm^{-1}.

Elemental analysis: N, 8.42, C, 47.98, H, 3.11

MS (ESI): m/z 274.9 (M - Cl), 276.9 (M - Cl), 275.9 (M - Cl)

3.2.2.7 Synthesis of Complex 7

An emulsion of 50 mg (2.19×10^{-4} mol) of ligand L_5 and 10 ml methanol was slowly added to a solution of 37 mg (2.19×10^{-4} mol) $CuCl_2 \cdot 2H_2O$ in 10 ml methanol. The resulting dark red reaction mixture was left unperturbed at room temperature for crystallization (slow evaporation of the solvent). Within a few weeks complex **7** was obtained as a black crystalline powder, which was washed with diethyl ether. Yield: 69%.

$C_{13}H_{11}ClCuN_2O_2$; Molecular Weight: 326,24

IR (neat) 3565, 2925, 1653, 1618, 1559, 1541, 1476, 1434, 1363, 1211, 1093, 851, 818, 775, 594 cm^{-1}.

Elemental analysis: N, 7.045±0.16263, C, 40.22±0.07071, H, 3.02±0.0
MS (ESI): m/z 324.98 (M), 326.98 (M), 328.27 (M), 330.03

3.2.2.8 Synthesis of Complex 8

An emulsion of 50 mg (2.01×10^{-4} mol) of ligand L_1 and 10 ml methanol was slowly added to a solution of 27 mg (2.01×10^{-4} mol) $ZnCl_2$ in 10 ml methanol. The resulting red reaction mixture was left unperturbed at room temperature for crystallization (slow evaporation of the solvent). Within a few weeks complex **8** was obtained as a red crystalline powder, which was washed with diethyl ether. Yield: 58%.
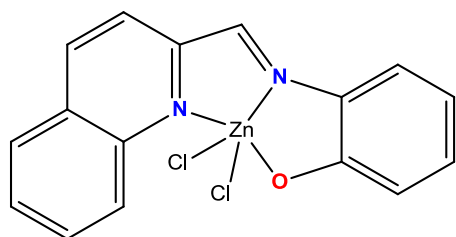
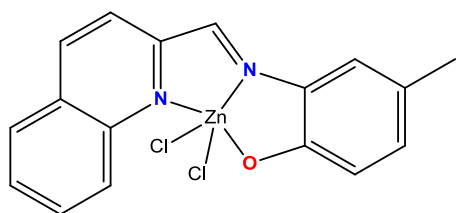$C_{16}H_{11}Cl_2N_2OZn$, Molecular Weight: 383.56.

IR (neat) 3435, 3220, 1587, 1508, 1475, 1462, 1304, 1255, 1148, 943, 835, 781, 754, 616 cm^{-1}.

Elemental analysis: N, 6.425±0.12, C, 49.95±0.11, H, 4.22±0.042.

MS (ESI): m/z 311.02 (M - Cl), 312.02 (M - Cl), 313.01 (M - Cl), 315.01 (M - Cl)

3.2.2.9 Synthesis of Complex 9

An emulsion of 50 mg (1.91×10^{-4} mol) of ligand L_2 and 10 ml methanol was slowly added to a solution of 26 mg (1.91×10^{-4} mol) $ZnCl_2$ in 10 ml methanol. The resulting dark brown reaction mixture was left unperturbed at room temperature for crystallization (slow evaporation of the solvent). Within a few weeks complex **9** was obtained as a red crystalline powder, which was washed with diethyl ether. Yield: 59%.

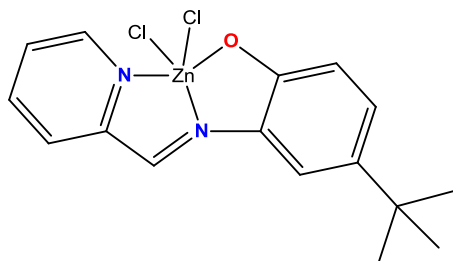$C_{17}H_{13}Cl_2N_2OZn$, Molecular Weight: 397,58.

IR (neat) 3412, 2360, 2341, 1637, 1615, 1584, 1508, 1486, 1461, 1435, 1382, 1295, 1259, 1236, 1217, 1151, 1138, 1009, 837, 816, 785, 768, 628, 487 cm^{-1}.

Elemental analysis: N, 7.79±0.051, C, 53.47±0.070, H, 3,13±0.046

MS (ESI): m/z 325.06 (M - Cl), 330.04 (M - Cl), 329.04 (M - Cl), 328.04 (M - Cl), 327.04 (M - Cl), 326.05 (M - Cl), 326.05 (M - Cl).

3.2.2.10   Synthesis of Complex 10

An emulsion of 50 mg (1.97×10^{-4} mol) of ligand L_3 and 10 ml methanol was slowly added to a solution of 27 mg (1.97×10^{-4} mol) $ZnCl_2$ in 10 ml methanol. The resulting dark red reaction mixture was left unperturbed at room temperature for crystallization (slow evaporation of the solvent). Within a few weeks complex **10** was obtained as a dark yellow crystalline powder, which was washed with diethyl ether. Yield: 62%.

$C_{16}H_{17}Cl_2N_2OZn$; Molecular Weight: 389.60.

m/z: 389.00 (100.0%), 387.00 (82.4%), 391.00 (43.2%), 390.99 (30.2%), 392.99 (25.2%), 390.00 (24.9%), 392.00 (16.8%), 388.00 (14.9%), 394.00 (4.7%), 394.99 (4.0%), 393.00 (3.1%), 389.01 (1.4%)

IR (neat) 3259, 3069, 2967, 2869, 1610, 1594, 1516, 1505, 1476, 1372, 1296, 1286, 1264, 1229, 1018, 821, 768, 632, 511 cm^{-1}.

Elemental analysis: N, 7.12±0.0, C, 49.10±0.02121, H, 4.675±0.00707

3.2.2.11   Synthesis of Complex 11

An emulsion of 50 mg (2.33×10^{-4} mol) of ligand L_4 and 10 ml methanol was slowly added to a solution of 32 mg (2.33×10^{-4} mol) $ZnCl_2$ in 10 ml methanol. The resulting dark red reaction mixture was left unperturbed at room temperature for crystallization (slow evaporation of the solvent). Within a few weeks complex **11** was obtained as a black crystalline powder, which was washed with diethyl ether. Yield: 49%.
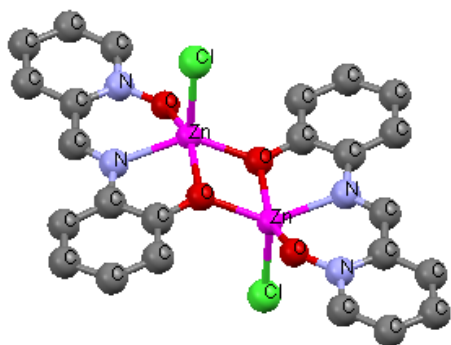
$C_{24}H_{18}Cl_2Zn_2N_4O_4$, Molecular Weight: 628,09.

IR (neat) 3437, 1587, 1487, 1469, 1433, 1316, 1282, 1257, 1205, 1181, 1146, 827, 759, 607, 556, 513, 471 cm^{-1}.

Elemental analysis: N, 8.67±0.064, C, 45.98±0.021, H, 2.80±0.036

**MS (Maldi-TOF)**: m/z 276.9 (M - Cl), 280.9 (M - Cl), 278.9 (M - Cl)

3.3. DNA binding studies

3.3.1. DNA cleavage

The efficiency of cleavage of these molecules was monitored using plasmidic DNA, pBR322, by agarose gel electrophoresis according to the established procedures [39, 50]. When pBR322 is subject to electrophoresis, the intact supercoil form will have a relatively fast migration (Form I). If scission occurs on one strand (nicking), the supercoil will relax to generate a slower-moving open circular form (Form II). If both strands are cleaved, a

linear form (Form III) migrates between Form I and Form II. In Figure 8 it is showed a schematic representation of these three forms and it relative migration. With this technique we can measure the amount of form II and III formed and the disappearance of the form I as we show in Figure 8.
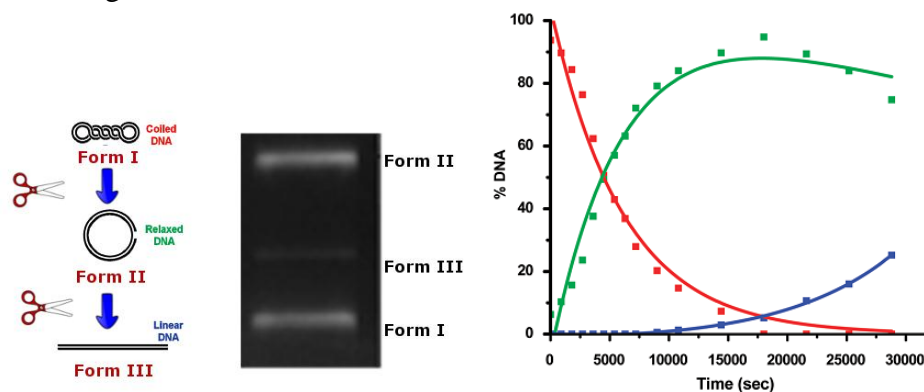
Figure 8: Schematic figure of forms I, II and III of DNA after DNA cleavage end respective Electrophoresis image. On the right we have a graphic representation of de disaperance of form I and consequent appearance of form II and II with time (Adapted from [51]).

All the stock solutions of the complexes (5 mM) in milli-Q water with 2% DMSO were freshly prepared before use.

The cleavage of pBR322 plasmid DNA (35 µg.mL^{-1}) was accomplished by the addition of different concentrations of complexes in Buffer (10 mM TE) at pH 7.4, incubated at 37 ℃ for 24h. All of the Cu(II) complexes were incubated 1h at 37ºC with reductant (5 mM 3-Mercaptopropionic acid). The reactions were quenched by the addition of 4 µl xylene. The mixtures were electrophoretized in agarose gel (1% a in 0.5 M TBE-Buffer for 5 h at 1,5 V.cm^{-1}.

Afterward, the DNA was dyed SYBR® dye and the images were taken.

3.3.2. Fluorescence spectroscopy

Competitive studies performed using ethidium bromide as a fluorescence probe is routinely used due to its sensitivity. EtBr is not fluorescent *per* se since it is quenched by solvent molecules but when intercalated with DNA it emits intense fluorescence at about 600 nm. This is due to its strong intercalation behavior between the adjacent DNA base pairs (stacking interactions), and this enhanced fluorescence could be quenched by the addition of another molecule. Competitive studies are based on the addition of a second molecule to compete with the intercalating EtBr for binding to DNA, so a reduction in the binding sites of DNA available for EtBr will result in a decrease of fluorescence [25].

The fluorescence assays was performed according with literature [52, 53]. To a 50 mg mL^{-1} CT DNA in TE, 30 µL of a 75 µM ethidium bromide solution and the mixture was incubated for 30 min at 37 °C. Increasing amounts of a 1.5 mM DMSO/Milli-Q water stock solution of the complex under study were added to reach the following final

concentrations of the complex: 0, 10, 20, 30, 40 and 50 μM with 24h incubation at 37 °C. Afterwards, the Fluorescence spectra (λ_{ex}=514 nm) were recorded at room temperature with a HORIBA Nanolog iHR 320 spectrophotometer in the wavelength range 530–800 nm.

3.3.3. Viscosity measurements

The interactions between the complex and DNA were investigated by viscosity measurements. Hydrodynamic measurements are sensitive to length change (i.e., viscosity and sedimentation) of DNA. We can detect the small changes caused by DNA complex interactions. A classical intercalation model usually resulted in lengthening the DNA helix, as base pairs were separated to accommodate the binding ligand leading to the increase of DNA viscosity, where as non-classical intercalation mode usually results in static bend or kink in the helix and decreases the viscosity of DNA [54].

The viscosity experiments were conducted at a constant temperature in a thermostatic bath 25 °C. Stock solutions of each complex were prepared in 2% DMSO/water. A 20 mg mL^{-1} CT DNA solution was prepared in TE buffer. For each complex increasing amounts of complex stock solution were added to this DNA solution to reach final concentrations of the complex: 0, 10, 20, 30, 40 and 50 μM. After a 24h incubation at 37 °C the viscosity of each sample was repeatedly measured. Mean values of five measurements performed at intervals of 1 min were used to evaluate the viscosity of each sample.

3.3.4.3.3.5. Atomic forces microscopy

Atomic force microscopy has been developed in and is becoming an essential tool in the visualization of biological interactions due to its astonishing high resolution allied to the simple sample preparation. These key factors allow it to be the technique that is ideally suited to the investigation of DNA structure and dynamics [55]. This is an analytical technique that provides "topographic" images by reflecting a laser from a probe that moves through the surface, and varies according to the atomic forces of electrostatic type will find in their path (in Figure 9 we can see a schematic image of the principles of AFM imaging and the respective tapping modes). The tapping mode allows an intermittent contact mode between the silicon tip and the sample, decreasing the error obtained by the damage cause by the constant screening of the sample. In this mode, a cantilever is deliberately vibrated at the frequency close to the cantilever resonant frequency by a piezoelectric modulator with very small amplitude. As the tip approaches the surface, the van der Waals attractive force between the tip and the sample changes both the amplitude and the phase of the cantilever vibration. These changes are monitored by a Z-servo system feed-back loop to control the tip–sample distance [56]. The binding of molecules to DNA leads to the distortion of its structure, but the extent of such distortion depends on the physical and chemical characteristics of the molecules and the forces between DNA and the molecules. AFM images of plasmid DNA allows us to see morphology of supercoiled DNA molecules and the respective alterations caused by binding molecules can be clearly observed. An illustration of how the intercalation changes the DNA structure is represented in the Figure 10.
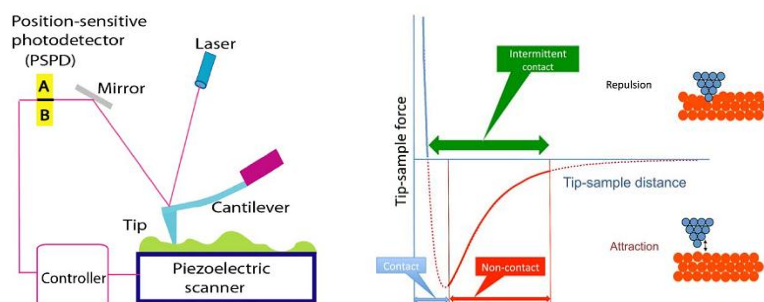
Figure 9: Schematic explaining the principles of AFM operation. On the left we can see a representation of the AFM tip (as a blue triangle) that reads the surface profile of the sample (shown in a green). The position of the tip relative to the sample is controlled by a piezoelectric scanner. On the right image we have a schematic representations of the different tapping modes (Adapted from [56]).

Solutions of metal complexes were prepared preciously through 0.2 nm FP030/3 filters (Scheicher and Schuell, Germany). The incubation samples were prepared with DNA pBR322 (0,25 µg.μL^{-1}), buffer HEPES and 75×10^{-3} µg.mL^{-1} of complex were prepared. After a 24h incubation at 37 °C all of the Cu(II) complexes were incubated 1h at 37ºC with reductant (5 mM 3-Mercaptopropionic acid). Afterwards, an AFM measurement was performed. Samples were prepared by placing a drop 5 µl of DNA solution or DNA and compound solution onto mica (Ted Pella, Inc. California, USA). After adsorption for 3 min at room temperature, the samples were rinsed for 10 s in a jet of deionized water directed onto the surface. The samples were blow dried with compressed argon and then imaged by AFM. The samples were imaged by a Nanoscope III Multimode AFM operating in tapping mode in air at RT operating in tapping mode.
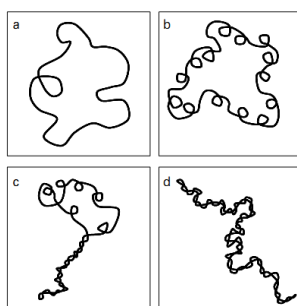

Figure 10: Illustration of the transitions in plasmid DNA tertiary structure in response to intercalation: (a) predominantly relaxed; (b) toroidally supercoiled; (c) mixed toroidal and plectonemic supercoils; (d) complete plectonemic supercoiling. Adapted from [55].

# Chapter IV: Results and discussion

4.1. X-ray structure

The only x-ray structures that were possible to determine were copper complex 4 and zinc complexes 8, 9 10 and 11.

The copper complex presented a mixture of the mononuclear (Figure 12) and a dinuclear (Figure 11) in solution. The first one is composed by one ligand coordinated to copper and the second one is composed by two copper centered. The bond angles are presented in the Table 2
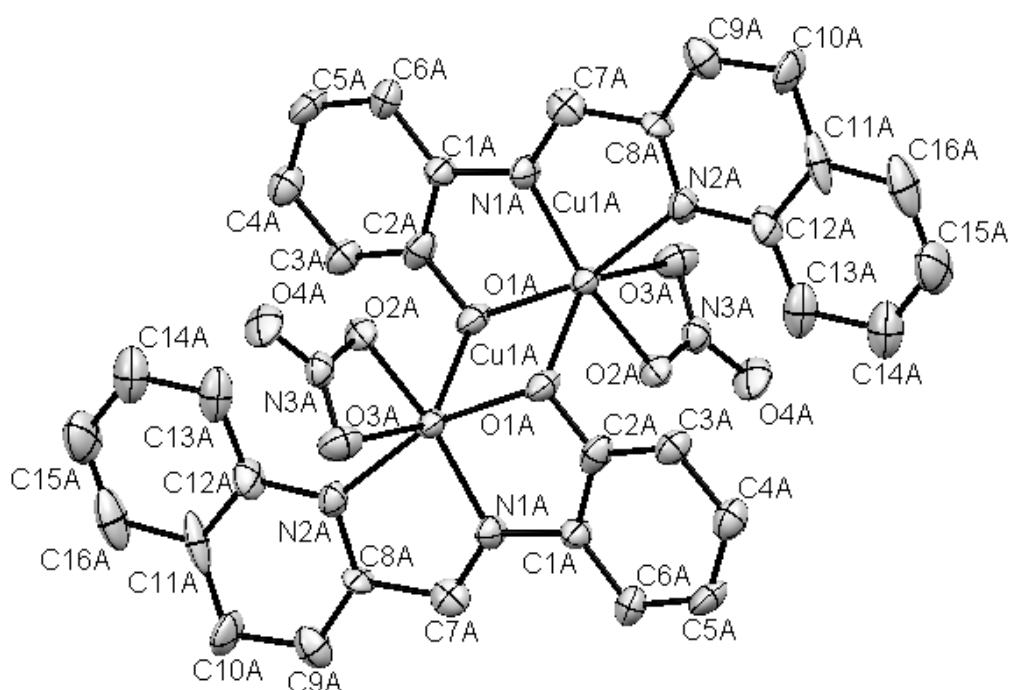
Figure 11: Crystallographic structure of crystal of complex 4 formed by two ligands coordinated to two Cu(II).
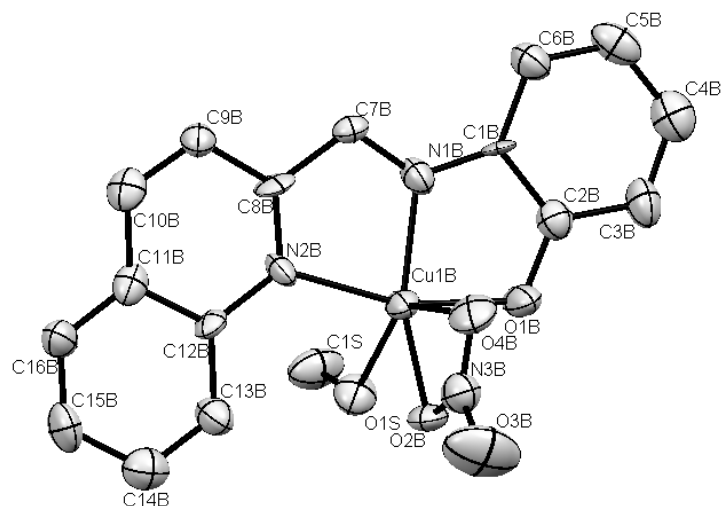
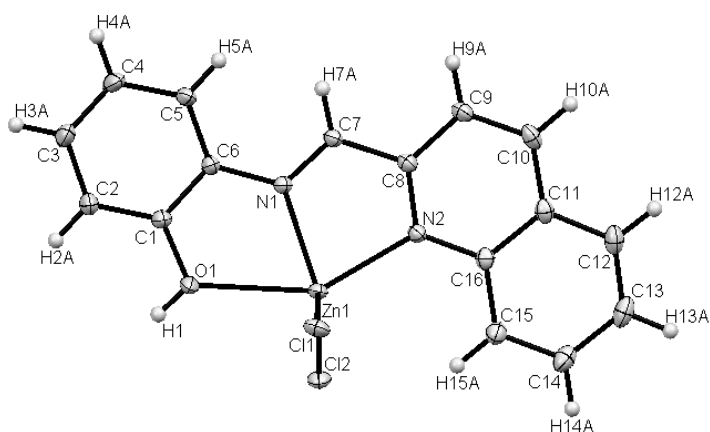**Figure 12: Crystallographic structure pf crystal of complex 4 formed by one ligand coordinated to the Cu(II).**

Table 1: Crystallographic data for the complex 4

Complex 4	
Formula	$C_{32}H_{22}Cu_2N_6O_8$, $C_{16}H_{11}CuN_3O_4$
Space Group	P -1
Cell Lengths	a 7.912(4) b 12.420(6) c 16.563(8)
Cell angles	α 79.089(9) β 76.276(9) γ 87.487(9)
Cell volume	1552.54

Table 2: Bond angles for the complex 4

Atom1	Atom2	Atom3	Angle	Atom1	Atom2	Atom3	Angle
O1A	Cu1A	N1A	83.9(4)	N1A	Cu1A	O3A	104.7(4)
O1A	Cu1A	N2A	162.9(4)	N2A	Cu1A	O2A	100.9(4)
O1A	Cu1A	O2A	94.4(4)	N2A	Cu1A	O3A	85.4(4)
O1A	Cu1A	O3A	97.7(4)	O2A	Cu1A	O3A	53.7(4)
O1A	Cu1A	O1A	80.6(3)	Cu1A	O1A	Cu1A	99.4(4)
N1A	Cu1A	N2A	79.1(4)	Cu1A	O1A	C2A	115.7(8)
N1A	Cu1A	O2A	158.0(4)	Cu1A	O1A	C2A	109.4(8)
N1A	Cu1A	O3A	104.7(4)	Cu1A	N1A	C1A	113.6(8)
N1A	Cu1A	O1A	113.0(4)	Cu1A	N1A	C7A	119.4(9)
N2A	Cu1A	O2A	100.9(4)	C1A	N1A	C7A	126(1)
N2A	Cu1A	O3A	85.4(4)	Cu1A	N2A	C8A	112.5(9)
N2A	Cu1A	O1A	107.3(4)	Cu1A	N2A	C12A	131.6(9)
O2A	Cu1A	O3A	53.7(4)	O1B	Cu1B	N1B	82.3(5)
O2A	Cu1A	O1A	88.2(4)	O1B	Cu1B	N2B	163.6(4)
O3A	Cu1A	O1A	141.8(3)	O1B	Cu1B	O1S	94.7(4)
Cu1A	O1A	C2A	109.4(8)	O1B	Cu1B	O2B	93.1(4)
Cu1A	O1A	Cu1A	99.4(4)	O1B	Cu1B	O4B	88.2(4)
C2A	O1A	Cu1A	115.7(8)	N1B	Cu1B	N2B	81.4(5)
Cu1A	N1A	C1A	113.6(8)	N1B	Cu1B	O1S	132.9(5)
Cu1A	N1A	C7A	119.4(9)	N1B	Cu1B	O2B	142.0(4)
Cu1A	N2A	C8A	112.5(9)	N1B	Cu1B	O4B	90.4(4)
Cu1A	N2A	C12A	131.6(9)	N2B	Cu1B	O1S	96.2(4)
Cu1A	O2A	N3A	108.5(7)	N2B	Cu1B	O2B	100.0(4)
Cu1A	O3A	N3A	78.2(7)	N2B	Cu1B	O4B	92.2(4)
O1A	Cu1A	O1A	80.6(3)	O1S	Cu1B	O2B	85.0(4)
O1A	Cu1A	N1A	113.0(4)	O1S	Cu1B	O4B	136.6(4)
O1A	Cu1A	N2A	107.3(4)	O2B	Cu1B	O4B	51.6(4)
O1A	Cu1A	O2A	88.2(4)	Cu1B	O1B	C2B	112.9(9)
O1A	Cu1A	O3A	141.8(3)	Cu1B	N1B	C1B	114.4(9)
O1A	Cu1A	N1A	83.9(4)	Cu1B	N1B	C7B	116.6(9)
O1A	Cu1A	N2A	162.9(4)	Cu1B	N2B	C8B	110.5(9)
O1A	Cu1A	O2A	94.4(4)	Cu1B	N2B	C12B	128.9(9)
O1A	Cu1A	O3A	97.7(4)	Cu1B	O1S	C1S	124(1)
N1A	Cu1A	N2A	79.1(4)	Cu1B	O2B	N3B	108.0(9)
N1A	Cu1A	O2A	158.0(4)	Cu1B	O4B	N3B	80.6(8)

Both zinc (II) complexes 8 and 9 (Figure 13 and Figure 14) present distorted trigonal bipyramid geometry formed by the oxygen (O1) and nitrogen (N1, N2) atoms of the ligand and two chloride ligands. The bond angles are presented in Table 4 and Table 6, respectively.
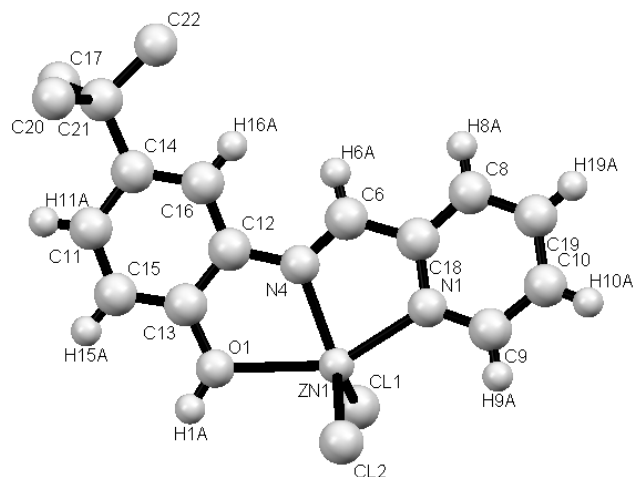
Figure 13: Crystallographic structure of the complex 8

Table 3: Crystallographic data for the complex 8

Complex 8	
Formula	$C_{16}H_{12}Cl_2N_2OZn$
Space Group	P 2_1/c
Cell Lengths	a 17.731(4) b 9.181(2) c 9.577(2)
Cell angles	α 90.00 β 105.01(3) γ 90.00
Cell volume	1505.83

Table 4:Bond angles for the complex 8

Atom1	Atom2	Atom3	Angle
Cl1	**Zn1**	Cl2	114.27(2)
Cl1	**Zn1**	O1	99.42(4)
Cl1	**Zn1**	N1	105.17(4)
Cl1	**Zn1**	N2	102.93(4)
Cl2	**Zn1**	O1	86.42(4)
Cl2	**Zn1**	N1	136.59(4)
Cl2	**Zn1**	N2	108.56(4)
O1	**Zn1**	N1	69.47(5)
O1	**Zn1**	N2	144.48(5)
N1	**Zn1**	N2	78.18(6)
Zn1	O1	H1	135(2)
Zn1	O1	C1	113.4(1)
Zn1	N1	C6	123.5(1)
Zn1	N1	C7	114.6(1)
Zn1	N2	C8	112.1(1)
Zn1	N2	C16	129.5(1)
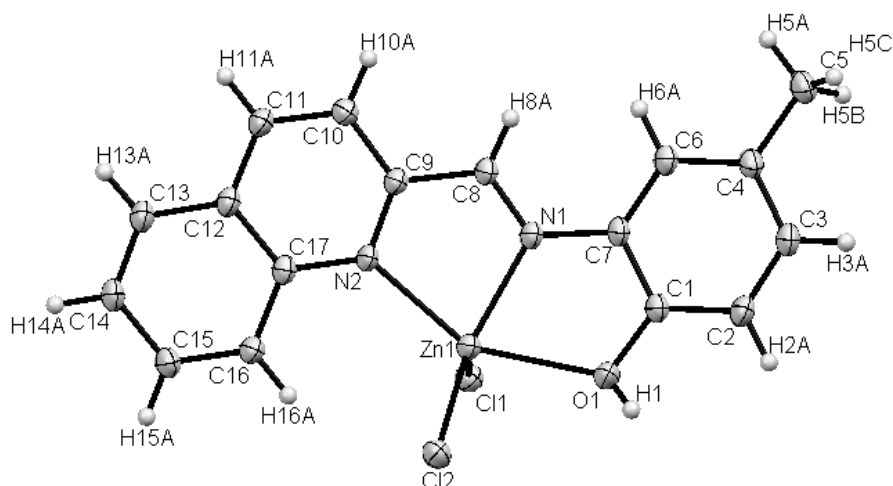
Figure 14: Crystallographic structure of the complex 9

Table 5: Crystallographic data for the complex 9

Complex 9	
Formula	$C_{17}H_{12}Cl_2N_2OZn$, CH_4O
Space Group	P -1
Cell Lengths	a 6.9590(14) b 8.892(2) c 14.817(3)
Cell angles	α 100.52(3) β 94.98(3) γ 100.87(3)
Cell volume	878.275

Table 6: Bond angles for the complex 9

Atom1	Atom2	Atom3	Angle
Cl1	**Zn1**	Cl2	114.13(3)
Cl1	**Zn1**	O1	99.51(5)
Cl1	**Zn1**	N1	105.17(6)
Cl1	**Zn1**	N2	102.03(6)
Cl2	**Zn1**	O1	86.36(5)
Cl2	**Zn1**	N1	137.68(6)
Cl2	**Zn1**	N2	107.41(6)
O1	**Zn1**	N1	71.90(7)
O1	**Zn1**	N2	146.54(7)
N1	**Zn1**	N2	77.91(8)
Zn1	O1	H1	137(3)
Zn1	O1	C1	113.7(2)
Zn1	N1	C7	122.0(2)
Zn1	N1	C8	114.7(2)
Zn1	N2	C9	110.3(2)
Zn1	N2	C17	130.7(2)

The zinc (II) complex 10 also presents a distorted trigonal bipyramid geometry (as presented in Figure 15) formed by the oxygen (O1) and nitrogen (N1 and N4) atoms of the ligand and two chloride ligands and the bond angles are presented in Table 8.

Figure 15: Crystallographic structure of the complex 10

Table 7: Crystallographic data for the complex 10

Complex 10	
Formula	$C_{17}H_{13}Cl_2N_2OZn$
Space Group	P -1
Cell Lengths	a 7.537(5) b 8.776(5) c 12.787(5)
Cell angles	α 74.274(5) β 85.887 (5) γ 88.725(5)
Cell volume	812.033

Table 8: Bond angles for the complex 10

Atom1	Atom2	Atom3	Angle
CL2	ZN1	CL1	114.81
CL2	ZN1	N4	129.02
CL2	ZN1	O1	94.81
CL2	ZN1	N1	100.12
CL1	ZN1	N4	115.34
CL1	ZN1	O1	95.77
CL1	ZN1	N1	102.48
N4	ZN1	O1	71.72
N4	ZN1	N1	77.56
O1	ZN1	N1	148.75
ZN1	N4	C6	114.64
ZN1	N4	C12	121.99
ZN1	O1	H1A	123.45
ZN1	O1	C13	113.1
ZN1	N1	C9	129.43
ZN1	N1	C18	112.78

The zinc (II) complex 11 is a dinuclear complex formed by two ligands and two zinc metallic centers as presented in Figure 16. The zinc is coordinated to the ligands by the oxygen (O1 and O2) and nitrogen (N1) atoms of the ligand and one chloride ligands and the bond angles are presented in Table 10.
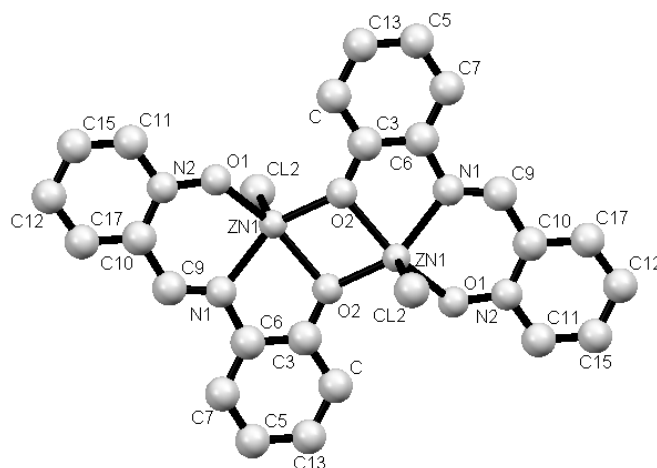
Figure 16: Crystallographic structure of the complex 11

Table 9: Crystallographic data for the complex 11

Complex 11	
Formula	$C_{24}H_{18}Cl_2Zn_2N_4O_4$, CH_4O
Space Group	$P\ 2_1/n$
Cell Lengths	a 9.3523(10) b 7.6245(8) c 17.6414(19)
Cell angles	α 90 β 101.062 γ 90
Cell volume	1234.58

Table 10: Bond angles for the complex 11

Atom1	Atom2	Atom3	Angle	Atom1	Atom2	Atom3	Angle
CL2	ZN1	O1	99.8	O2	ZN1	CL2	110.88
CL2	ZN1	O2	105.77	O2	ZN1	O1	100.47
CL2	ZN1	N1	106.92	O2	ZN1	O2	77.77
CL2	ZN1	O2	110.88	O2	ZN1	N1	139.61
O1	ZN1	O2	153.26	CL2	ZN1	O1	99.8
O1	ZN1	N1	86.43	CL2	ZN1	O2	105.77
O1	ZN1	O2	100.47	CL2	ZN1	N1	106.92
O2	ZN1	N1	78.83	O1	ZN1	O2	153.26
O2	ZN1	O2	77.77	O1	ZN1	N1	86.43
N1	ZN1	O2	139.61	O2	ZN1	N1	78.83
ZN1	O1	N2	125	ZN1	O1	N2	125
ZN1	O2	C3	114.15	ZN1	O2	ZN1	102.23
ZN1	O2	ZN1	102.23	ZN1	O2	C3	134.43
C3	O2	ZN1	134.43	ZN1	O2	C3	114.15
ZN1	N1	C6	112.48	ZN1	N1	C6	112.48
ZN1	N1	C9	124.14	ZN1	N1	C9	124.14

4.2. DNA binding studies

4.2.1 DNA cleavage

Electrophoresis is a useful technique to investigate DNA cleavage since we can see the different conformations of plasmid pBR322 DNA - supercoiled (form I), nicked DNA (form II) and linear DNA (form III). The electrophoresis images are presented in the supplementary information (Figure S 1 to Figure S 10).

The delivery of the metal ion to the helix, locally generating oxygen or hydroxide radicals, yields an efficient DNA cleavage reaction. In the present work we could not correctly optimize the technique, in order to take advantage of their full potential, and as a consequence we could not measure the quantity of form II and III originated. Despite this, the results were shown as complementary information. We cannot distinguish the isolated forms, but we can observe the appearance of bands with different length, and consequently

different electrophoretic mobilities (given by the velocity of charged species gained under unit electric field strength). This parameter depends on the physical and chemical properties of charged species and the medium. If the complexes have unspecific nuclease activities, we will see the formation of different bands. These bands will be more or less separated according to the time and the applied voltage.

Supercoiled DNA moves faster because of its tightest conformation that results in lower resistance on gel. With a slight change of its configuration, the electrophoretic mobility increases rapidly. Simultaneously, nicked DNA is the slowest since it occupies the biggest volume.

The different DNA cleavage efficiencies of the complexes is a consequence to the different binding affinity of the complexes to DNA. For complexes 1 and 2 we can observe a decrease of form I and the subsequent increasing amounts of nicked forms with a lower or higher electrophoretic mobility. In case of complex 1 the incubation with 200 μM of complex and complex 2 higher than 30 μM we can observe the complete degradation of DNA. These differences in the nuclease activity exhibited may be explained by the absence of the methyl group at the para position of the phenolic ring. The methyl group, may help the formation and stabilization of a phenoxyl radical, which obviously plays an important part in the DNA cleavage (through a radical pathway) increasing cleavage ability. Other examples are complexes 6 and 7. In this case we also can see a similar effect, the last one having a more effective nuclease activity.

Copper compounds are known by their oxidative DNA damage. For Zinc compounds we can evidence complexes 10 and 11. They also present a nuclease behavior with the formation of different bands with distinct electrophoretic mobilities.

4.2.2 Fluorescence spectroscopy

Fluorescence measurements were recorded in order to identify the interaction modes of our study complexes with DNA. The emission intensity of EtBr bound to CT-DNA has been measured in the presence of different concentrations of Cu(II) and Zn(II) complexes. If the complexes attend to compete with EtBr, if the replacement occurs, the fluorescence decreases. Due to the planar structures of the complexes it was expected that complexes efficiently replace EtBr at the intercalating binding sites of DNA with stronger binding affinities

The individual fluorescence quenching curves when incubated 24h with each complex can be found in the supporting information (Figure S 11to Figure S 21).

In Figure 17 are presented all of the complexes and their quenching abilities when incubated 24h with CT-DNA.
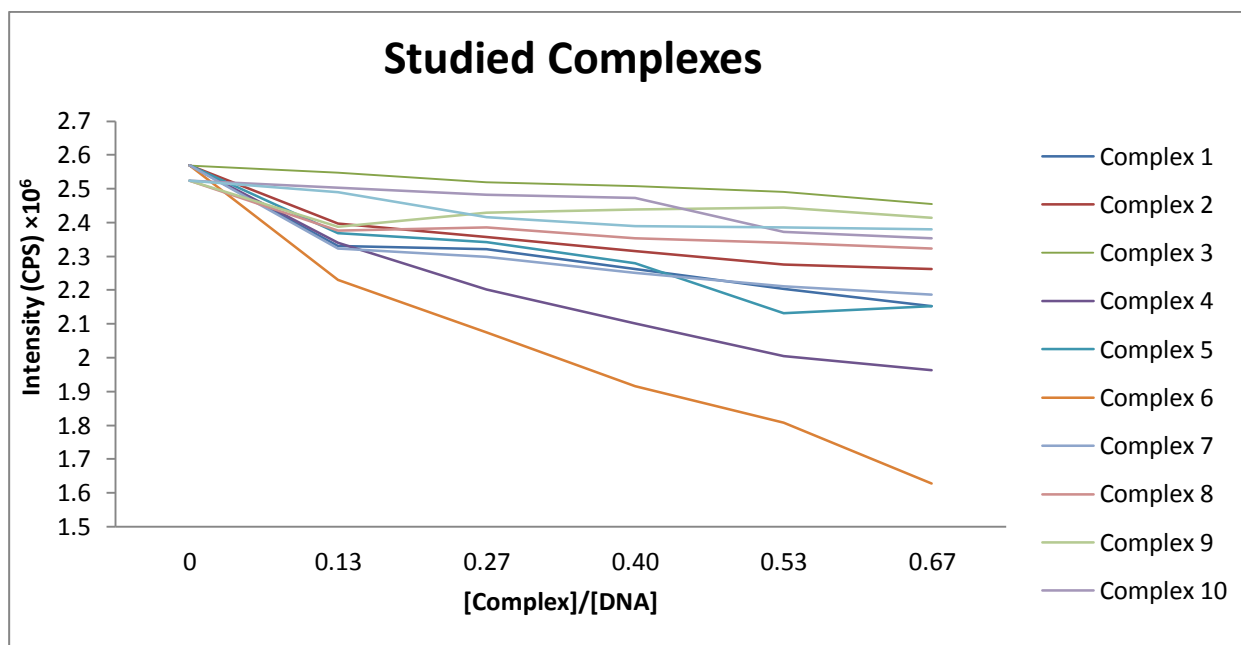
Figure 17: Differences in fluorescence quenching curves of EB bound to DNA by the studied complexes ([complex] = 0–50 μM). In this its represented the decreasing of the maximum intensity vs [Complex]/[DNA] (ri).
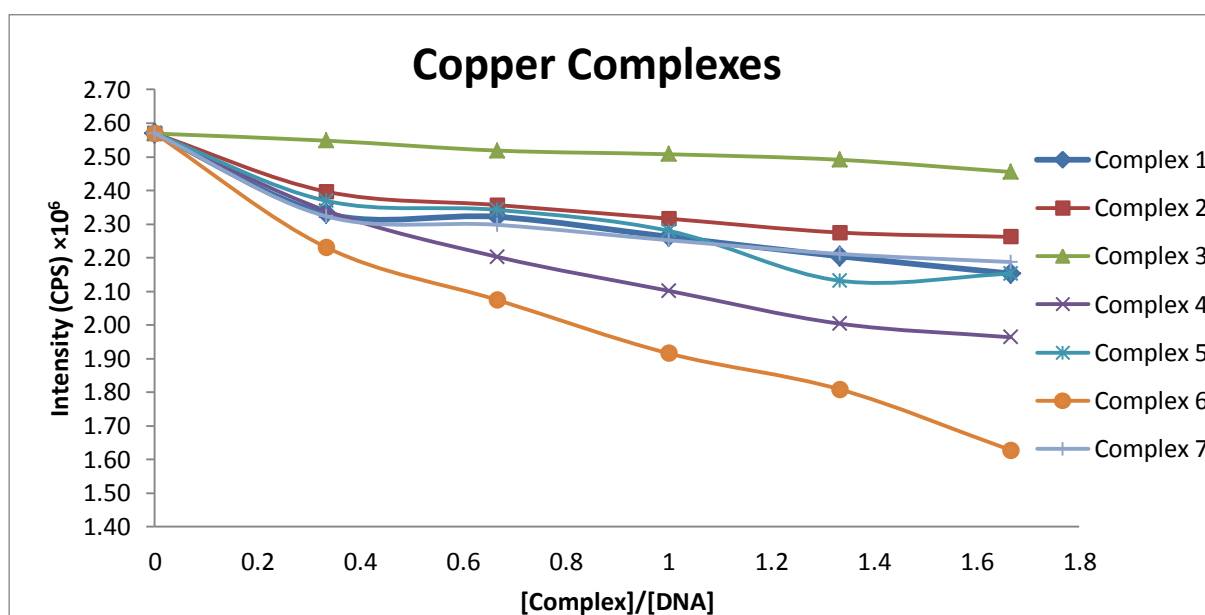
Figure 18: Differences in fluorescence quenching curves of EB bound to DNA by copper complexes ([complex] = 0–50 μM). In this its represented the decreasing of the maximum intensity vs [Complex]/[DNA] (ri).

In the Figure 18: Differences in fluorescence quenching curves of EB bound to DNA by copper complexes ([complex] = 0–50 μM). In this its represented the decreasing of the maximum intensity vs [Complex]/[DNA] (ri).Figure 18 we have represented the summary of the decreasing of the maximum intensity lead by the studied copper. In this

range of concentrations, copper complexes present a linear intercalation behavior. Complex 6 presents the stronger ability to replace the EtBr, quenching about 30% of the fluorescence when the proportion is approximately 0.5:1 (Complex: DNA), this should also be verified in Figure S 16. The ability to bind efficiently DNA are Complex 6 (30%)> Complex 4 (22%) > Complex 5 (17%)> complex 7 (14)> Complex 1 (14%) > Complex 2 (11%) > Complex 3 (3%).

The structure of the complex 6 allows it to intercalate more efficiently and consequently the better quencher character. The complex 4 is constituted by a mononuclear and a dinuclear complex and this could be a reason for the quenching ability, lower than the first complex, but also a significant one. Also the structure of complex 5 and 7 allows good intercalation ability, but the introduction of the metil group can destabilize the complex. They present an steric impediment to the intercalation ability. We also can apply the same principle to complexes 2 and 3, the complexes with the worst quenching abilities, comparatively with all other complexes.
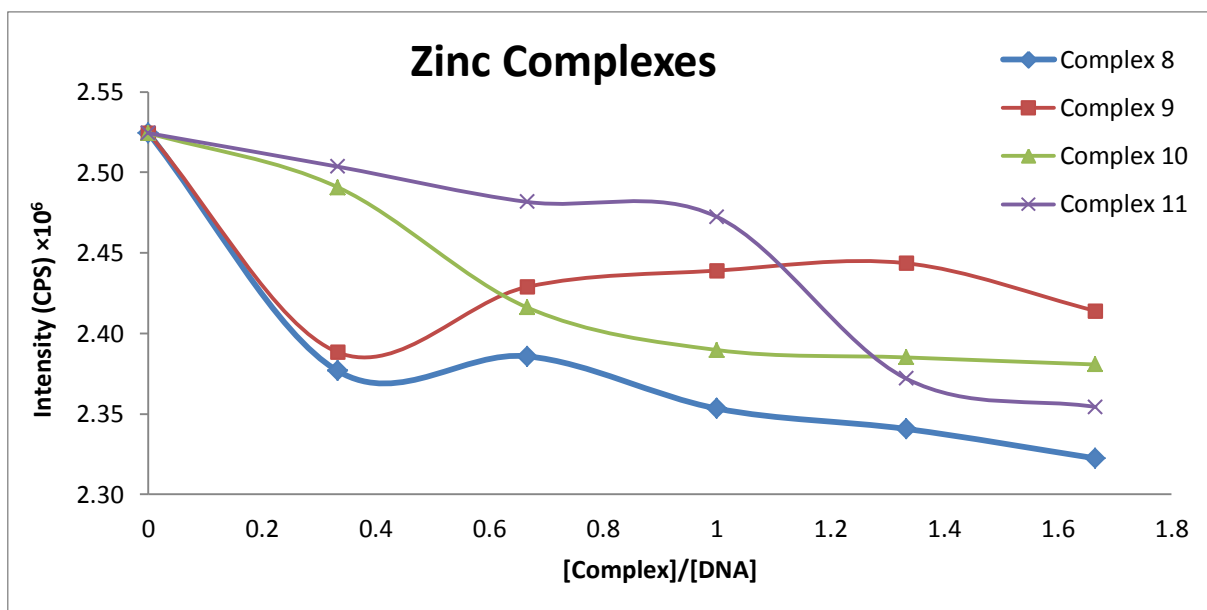
Figure 19: Differences in fluorescence quenching curves of EB bound to DNA by Zinc complexes ([complex] = 0–50 μM). In this its represented the decreasing of the maximum intensity vs [Complex]/[DNA] (ri).

Figure 19 represents a summary of the differences in the maximum intensity when DNA was incubated with the studied zinc complexes. Contrary to copper complexes, Zn(II) complexes do not present a linear intercalation behavior. The intercalation is not significative when compared to Cu(II) complexes. The complex that presents a stronger ability to replace the EtBr, in this case is Complex 8, quenching in about 7.28% of the fluorescence when the proportions approximately 0.5:1 (Complex: DNA). It is followed by Complex 10 (6.04%)> Complex 11 (5.52%) > Complex 9 (3.20%).

The structure has a main role in the intercalation behavior, and comparatively to complex 1 (14% of quenching, with the same ligand), we can conclude that Zn(II) promotes weaker interactions with DNA having a lower affinity with Cu(II). This is also valid for complex 9 and complex 2 (11% of quenching, with the same ligand).

4.2.3 Viscosity measurements

To further clarify the nature of the interactions between the different complexes and DNA viscosity measurements were carried out by varying the complex concentrations (0-50 µM) added to CT-DNA. When intercalation takes place, we expect the lengthen of the DNA helix as the base pairs are pushed apart in order to accommodate the bound ligand. This leads to and increasing in the DNA viscosity. Whereas if a partial, non-classical ligand intercalation or outside binding occurs, the bending DNA helix decreases its efficient length and thereby the viscosity is diminished. In Figure 20 and Figure 21 it is represented the viscosity changes with the increase of the [Complex]/[DNA] ratio.

At the supporting information it is plotted the relative viscosity $(\eta/\eta_0)^{1/3}$ vs [Complex]/[DNA] ratio for each complex (Figure S 22 to Figure S 32). Those graphics do not have any conclusive remarks; they only show a possible tendency.

In Figure 20 we have the representation of all copper complexes and their influence on the viscosity when incubated 24h with CT-DNA.
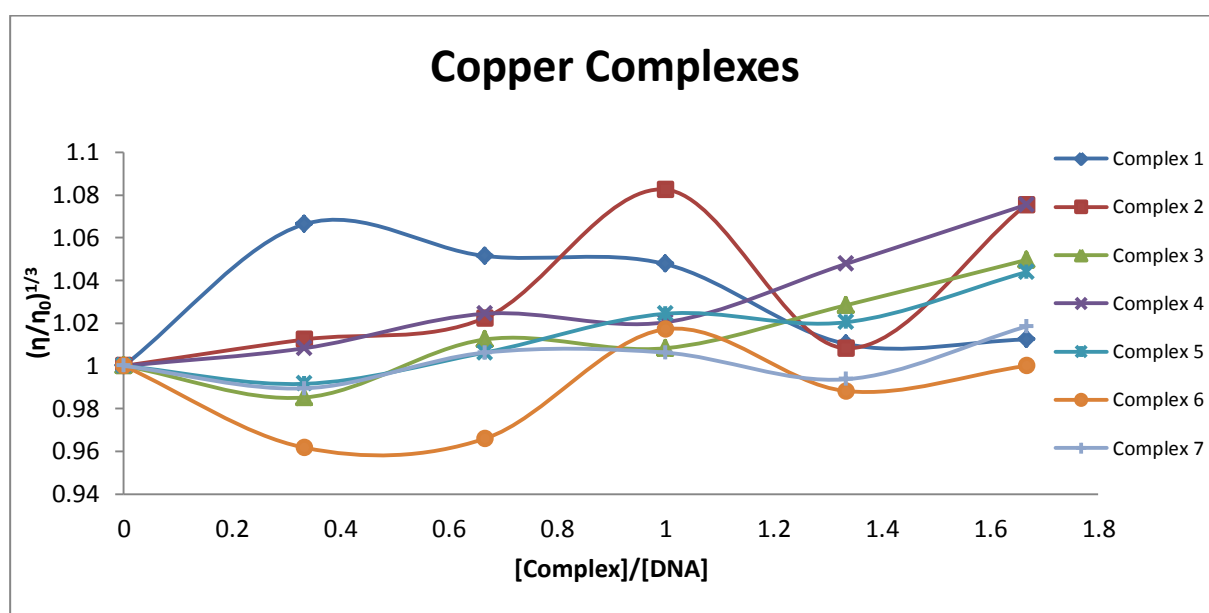
Figure 20: Representation of the viscosity data of the copper complexes with DNA.
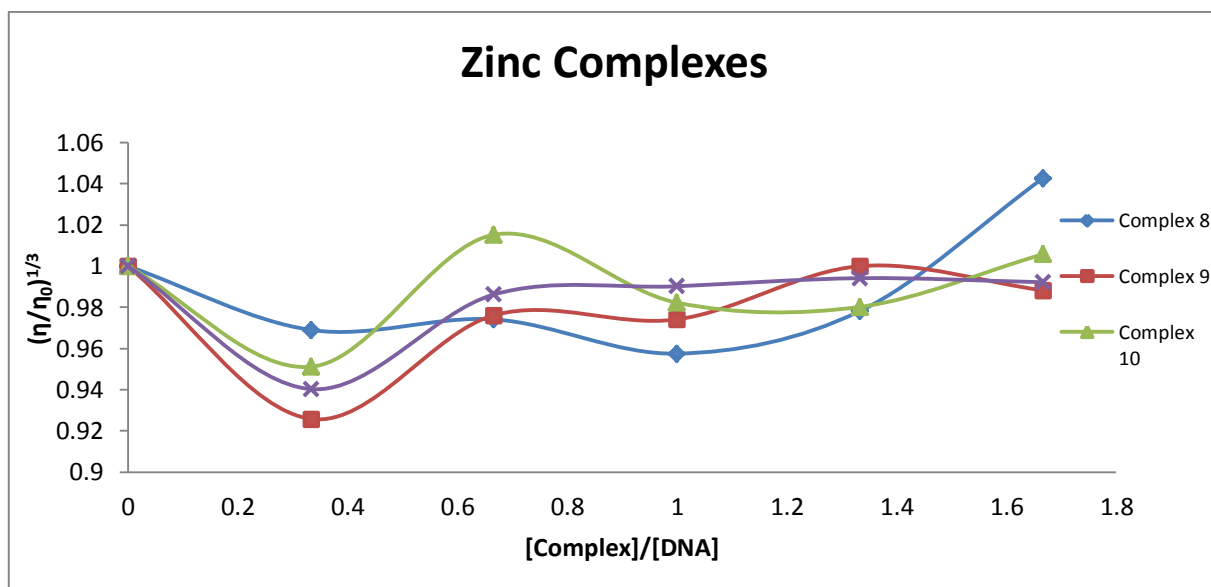
Figure 21: Representation of the viscosity data of the zinc complexes with DNA.

This information cannot be conclusive due to the oscillations of the viscosity. However, the results confirm the deductions been made so far. We can evidence an increasing (in some cases linear) in the viscosity in all the complexes, except for complex 1. In this case we can see the decrease in the viscosity and this interaction leads us to think that the interaction of this complex with DNA results in the contraction of the DNA helix. On the other hand we have the increase of the viscosity (linear in most copper complexes) an indicator of the lengthening of the DNA helix.

Once again we can highlight the higher intercalation behavior of Cu(II) complexes when compared to the Zn(II). With this technique we cannot fully understand the interaction mode of the Zn(II).

4.2.4   Atomic forces microscopy

All the AFM images are presented in the supporting information (Figure S 33 to Figure S 46).

The effects on the tertiary structure of plasmid DNA in response to small molecule binding can be observed. The DNA adopted a fairly relaxed conformation, typically having only one or two strand crossovers and we represent it in Figure S 33. As showed in other analyses the reductant used in the assays does not damage the DNA. If we incubate the DNA with different molecules we will observe an increasing superhelical stress due to, for example, intercalation. We clearly observe a transition to a structure consisting of a series of toroidal supercoils (illustrated above on Figure 10). A further increase in stress can lead to the adoption of tightly interwound supercoiled regions alongside the toroidal supercoiling (as we can see in the complexes 10 and 11, Figure S 43 to Figure S 46).

Copper complexes showed an interesting intercalation properties allied to the well-known nuclease properties. We can clearly see it in the AFM images of complexes 1 and 2 (Figure S 34 and Figure S 35).

Compounds 10 and 11 reveled interesting properties, as it is showed that they interact with pBR322 forming "clusters". This fact contradicts the fluorescence measurements, because they didn't showed remarkable intercalation abilities.

These properties have to be further investigated in order to determine the type of DNA interaction, they can possibly be caused by some crosslink that destabilizes the DNA chain, generating tensions and leading to these interesting agglomerates. These extraordinary binding affinities can be an advantage in cancer research, so in order to fully understand it, more studies should be carried.

4.2.5 Further studies

For the complexes with a good intercalation behavior we can also determine the apparent binding constant (k_{app}) applying Stern-Volmer equation (performing the assays with a wide range of concentrations).

We also can perform circular dichroism in order to determine the DNA secondary structure interactions, essentially by the zinc complexes.

Electrophoresis studies have to be performed (and optimized) to further conclusions on the nuclease activity of the complexes.

Due to the excellent features of Schiff bases, Cu(II) and Zn (II) complexes there are a lot of possibilities for further studies with these complexes. The interaction of these complexes with proteins, such as cytochrome C, telomerase, topoisomerase enzyme or other protein complexes involved in the metabolism replication are also an interesting subject.

Chapter V: Conclusion

Medicinal inorganic chemistry is a discipline of an exponential growing interest due to the significance of metal complexes in both therapeutic and diagnostic medicine.

A novel series of tridentate Schiff bases were synthetized, containing N and O donor sets and corresponding Cu(II) and Zn(II) complexes have been obtained and characterized.

All the complexes showed interaction with DNA but the comparative DNA studies revealed that Cu(II) complexes have a better intercalation behavior when compared to the Zn (II), therefore they have a higher affinity for DNA intercalation.

The structure of the complexes allowed the formation and stabilization of the phenoxyl radical, enhancing the DNA cleavage in complex 2 and 7 (comparatively to 1 and 6 respectively).

AFM results showed that all complexes are able to modify significantly the tertiary structure of DNA. Despite the fluorescence results, we can see clearly the strong interaction of the Zn(II) complexes with DNA leading to an alteration in the tertiary structure. These remarkable binding interactions should be investigated in further work.

Finally, it is important to note that the cytotoxicity and anti-proliferative studies of these complexes are being undertaken.

Bibliography

[1] M.L. Turski, D.J. Thiele, J Biol Chem 284 (2009), 717-721.

[2] P. de Hoog, M.J. Louwerse, P. Gamez, M. Pitié, E.J. Baerends, B. Meunier, J. Reedijk, European Journal of Inorganic Chemistry 2008 (2008), 612-619.

[3] P.U. Maheswari, S. Roy, H. den Dulk, S. Barends, G. van Wezel, B. Kozlevčar, P. Gamez, J. Reedijk, Journal of the American Chemical Society 128 (2005), 710-711.

[4] S. Özalp-Yaman, P. de Hoog, P.U. Maheswari, H. Casellas, A. Golobic, B. Kozlevcar, P. Gamez, J. Reedijk, Electrochimica Acta 55 (2010), 8655-8663.

[5] J. Ferlay, H.R. Shin, F. Bray, D. Forman, C. Mathers, D.M. Parkin, in: I.A.f.R.o. Cancer (Ed.), IARC CancerBase vol. 10, GLOBOCAN, Lyon, France, 2010.

[6] C. Avendaño, J.C. Menéndez, Medicinal chemistry of anticancer drugs, 1st Ed, Elsevier, Amsterdam ; Boston, 2008. pp 1-7.

[7] R.C. Cattley, R.R. Radinsky, Toxicol Pathol 32 Suppl 1 (2004), 116-121.

[8] D. Hanahan, R.A. Weinberg, Cell 100 (2000), 57-70.

[9] M. Frezza, S. Hindo, D. Chen, A. Davenport, S. Schmitt, D. Tomco, Q. Ping Dou, Current Pharmaceutical Design 16 (2010), 1813-1825.

[10] C.H. Zhou, Y.Y. Zhang, C.Y. Yan, K. Wan, L.L. Gan, Y. Shi, Anticancer Agents Med Chem 10 (2010), 371-395.

[11] K. Gurova, Future Oncol 5 (2009), 1685-1704.

[12] R.W. Ruddon, Cancer biology, 4th Ed, Oxford University Press, Oxford ; New York, 2007. pp 3-14.

[13] H. Beinert, J Biol Chem 277 (2002), 37967-37972.

[14] T. Storr, K.H. Thompson, C. Orvig, Chem Soc Rev 35 (2006), 534-544.

[15] N. Farrell, Royal Society of Chemistry (Great Britain), Uses of inorganic chemistry in medicineEd, Royal Society of Chemistry, Cambridge, 1999. pp 1-9; 109-120.

[16] D. Gambino, Curr Med Chem 17 (2010), 3605.

[17] M.Z. Hernandes, S.P.F.J. de, L.C. Coelho, D.R. Moreira, V.R. Pereira, A.C. Leite, Curr Med Chem 17 (2010), 3739-3750.

[18] K. Ferrante, B. Winograd, R. Canetta, Cancer Chemotherapy and Pharmacology 43 (1999), S61-S68.

[19] J. Hirsch, JAMA: The Journal of the American Medical Association 296 (2006), 1518-1520.

[20] C.J. Lord, A. Ashworth, BMC Biol 8 (2010), 38.

[21] J.J.R.F.d. Silva, R.J.P. Williams, The biological chemistry of the elements : The inorganic chemistry of life, 2nd Ed, Oxford University Press, Oxford ; New York, 2001. pp 299-318, 388-399.

[22] D.D. Li, J.L. Tian, W. Gu, X. Liu, H.H. Zeng, S.P. Yan, J Inorg Biochem 105 (2011), 894-901.

[23] C. Marzano, M. Pellei, F. Tisato, C. Santini, Anti-Cancer Agents in Medicinal Chemistry (Formerly Current Medicinal Chemistry 9 (2009), 185-211.

[24] L.M. Mirica, X. Ottenwaelder, T.D. Stack, Chem Rev 104 (2004), 1013-1045.

[25] X. Qiao, Z.Y. Ma, C.Z. Xie, F. Xue, Y.W. Zhang, J.Y. Xu, Z.Y. Qiang, J.S. Lou, G.J. Chen, S.P. Yan, J Inorg Biochem 105 (2011), 728-737.

[26] F. Arjmand, M. Muddassir, Journal of Photochemistry and Photobiology B: Biology 101 (2010), 37-46.

[27] D.S. Sigman, Accounts of Chemical Research 19 (1986), 180-186.

[28] S.H. van Rijt, P.J. Sadler, Drug Discovery Today 14 (2009), 1089-1097.

[29] P. Gamez, I.W. Arends, J. Reedijk, R.A. Sheldon, Chem Commun (Camb) (2003), 2414-2415.

[30] S. van der Steen, P. de Hoog, K. van der Schilden, P. Gamez, M. Pitié, R. Kiss, J. Reedijk, Chemical Communications 46 (2010), 3568.

[31] P. Hoog, C. Boldron, P. Gamez, K. Sliedregt-Bol, I. Roland, M. Pitie, R. Kiss, B. Meunier, J. Reedijk, J Med Chem 50 (2007), 3148-3152.

[32] K. Singh, M.S. Barwa, P. Tyagi, Eur J Med Chem 41 (2006), 147-153.

[33] M. Shakir, A. Abbasi, A.U. Khan, S.N. Khan, Spectrochim Acta A Mol Biomol Spectrosc 78 (2011), 29-35.

[34] C. Spinu, A. Kriza, Acta Chem. Slov. 47 (2000), 179-185.

[35] F. Tisato, C. Marzano, M. Porchia, M. Pellei, C. Santini, Medicinal Research Reviews 30 (2010), 708-749.

[36] G. Parkin, Chem Rev 104 (2004), 699-767.

[37] W. Maret, Y. Li, Chemical Reviews 109 (2009), 4682-4707.

[38] T. Fukada, S. Yamasaki, K. Nishida, M. Murakami, T. Hirano, J Biol Inorg Chem 16 (2011), 1123-1134.

[39] P.U. Maheswari, S. Barends, S. Ozalp-Yaman, P. de Hoog, H. Casellas, S.J. Teat, C. Massera, M. Lutz, A.L. Spek, G.P. van Wezel, P. Gamez, J. Reedijk, Chemistry 13 (2007), 5213-5222.

[40] B.P. Joshi, W.-M. Cho, J. Kim, J. Yoon, K.-H. Lee, Bioorganic & Medicinal Chemistry Letters 17 (2007), 6425-6429.

[41] L.H. Hurley, Nat Rev Cancer 2 (2002), 188-200.

[42] M. Maiti, G.S. Kumar, Med Res Rev 27 (2007), 649-695.

[43] N.D. Hadjiliadis, E. Sletten, Metal complex - DNA interactions, 1st Ed, Wiley, Chichester, West Sussex, U.K., 2009. pp 1-26, 95-128, 135-164.

[44] M.S. Cooke, M.D. Evans, Science & Medicine 10 (2005), 98-111.

[45] S.M. Nelson, L.R. Ferguson, W.A. Denny, Cell Chromosome 3 (2004), 2.

[46] Q. Jiang, N. Xiao, P. Shi, Y. Zhu, Z. Guo, Coordination Chemistry Reviews 251 (2007), 1951-1972.

[47] W.K. Pogozelski, T.D. Tullius, Chem Rev 98 (1998), 1089-1108.

[48] C.J. Burrows, J.G. Muller, Chem Rev 98 (1998), 1109-1152.

[49] M. Brasse, J. Cámpora, P. Palma, E. Álvarez, V. Cruz, J. Ramos, M.L. Reyes, Organometallics 27 (2008), 4711-4723.

[50] A. Arbuse, M. Font, M.A. Martinez, X. Fontrodona, M.J. Prieto, V. Moreno, X. Sala, A. Llobet, Inorg Chem 48 (2009), 11098-11107.

[51] L. Tjioe, A. Meininger, T. Joshi, L. Spiccia, B. Graham, Inorg Chem (2011).

[52] J. Benítez, L. Becco, I. Correia, S.M. Leal, H. Guiset, J.C. Pessoa, J. Lorenzo, S. Tanco, P. Escobar, V. Moreno, B. Garat, D. Gambino, Journal of Inorganic Biochemistry 105 (2011), 303-312.

[53] S.S. Bhat, A.A. Kumbhar, H. Heptullah, A.A. Khan, V.V. Gobre, S.P. Gejji, V.G. Puranik, Inorg Chem (2010).

[54] M.N. Patel, M.R. Chhasatia, D.S. Gandhi, Bioorg Med Chem 17 (2009), 5648-5655.

[55] L.H. Pope, M.C. Davies, C.A. Laughton, C.J. Roberts, S.J.B. Tendler, P.M. Williams, Journal of Microscopy 199 (2000), 68-78.

[56] Y.L. Lyubchenko, Micron 42 (2011), 196-206.

Supporting Information

S1. Electrophoresis
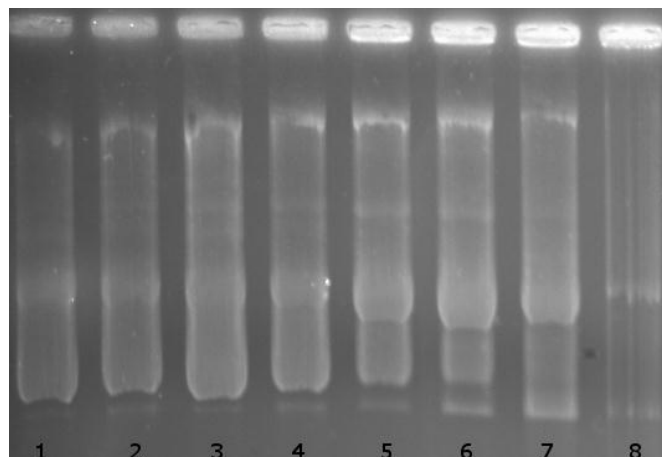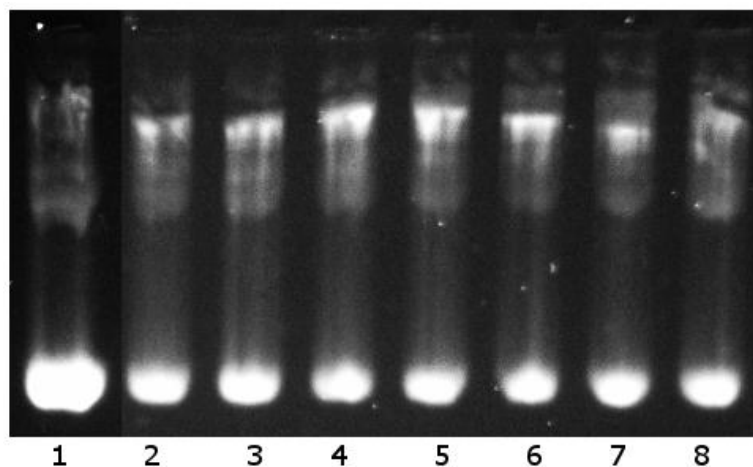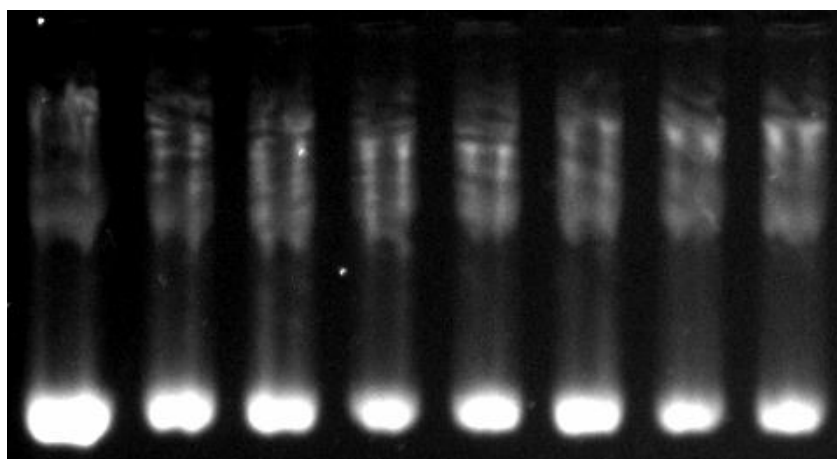

Figure S 1: Agarose gel showing cleavage of DNA (µgµL^{-1}) incubated with different concentrations of complex 1. Lane 1 DNA, Lane 2 DNA+10 µM, Lane 3 DNA+20 µM, Lane 4 DNA+30 µM, Lane 5 DNA+40 µM, Lane 6 DNA+50 µM, Lane 7 DNA+100 µM, Lane 8 DNA + 200 µM.
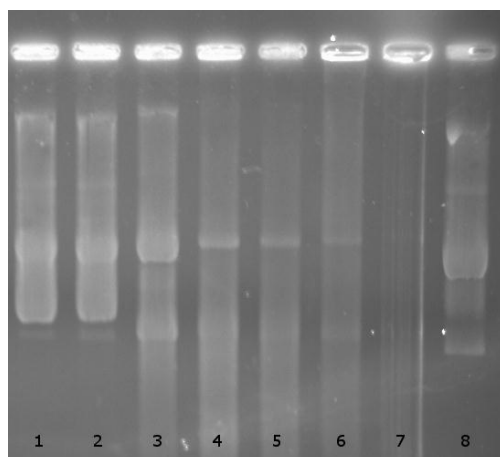
Figure S 2: Agarose gel showing cleavage of DNA (µgµL^{-1}) incubated with different concentrations of complex 2. Lane 1 DNA, Lane 2 DNA+10 µM, Lane 3 DNA+20 µM, Lane 4 DNA+40 µM, Lane 5 DNA+50 µM, Lane 6 DNA+100 µM, Lane 7 DNA+200 µM, Lane 8 DNA + 30 µM.
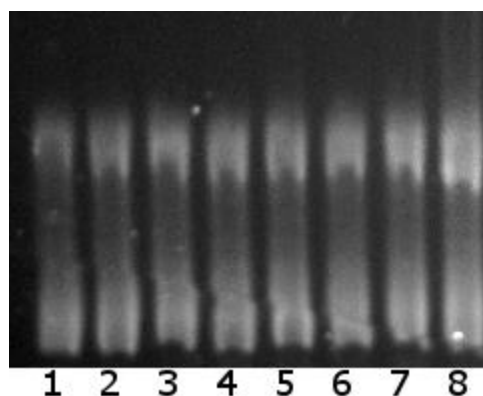
Figure S 3: Agarose gel showing cleavage of DNA (μgμL^{-1}) incubated with different concentrations of complex 3. Lane 1 DNA, Lane 2 DNA+10 μM, Lane 3 DNA+20 μM, Lane 4 DNA+30 μM, Lane 5 DNA+40 μM, Lane 6 DNA+50 μM, Lane 7 DNA+100 μM, Lane 8 DNA + 200 μM.
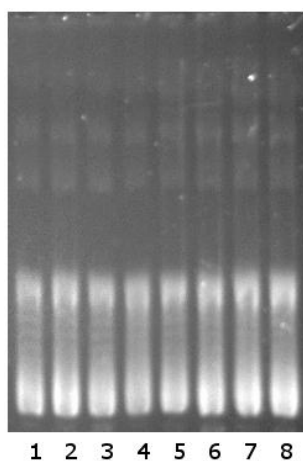
Figure S 4: Agarose gel showing cleavage of DNA (μgμL-1) incubated with different concentrations of complex 4. Lane 1 DNA, Lane 2 DNA+10 μM, Lane 3 DNA+20 μM, Lane 4 DNA+30 μM, Lane 5 DNA+40 μM, Lane 6 DNA+50 μM, Lane 7 DNA+100 μM, Lane 8 DNA + 200 μM.
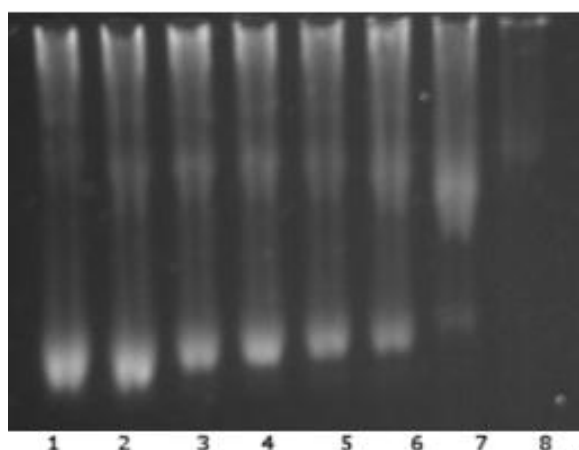
Figure S 5: Agarose gel showing cleavage of DNA (μgμL^{-1}) incubated with diferent concentrations of complex 6. Lane 1 DNA, Lane 2 DNA+10 μM, Lane 3 DNA+20 μM, Lane 4 DNA+30 μM, Lane 5 DNA+40 μM, Lane 6 DNA+50 μM, Lane 7 DNA+100 μM, Lane 8 DNA + 200 μM.
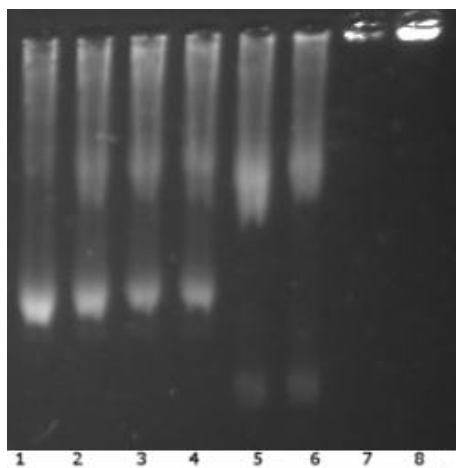
Figure S 6: Agarose gel showing cleavage of DNA (µgµL^{-1}) incubated with diferent concentrations of complex 7. Lane 1 DNA, Lane 2 DNA+10 µM, Lane 3 DNA+20 µM, Lane 4 DNA+30 µM, Lane 5 DNA+40 µM, Lane 6 DNA+50 µM, Lane 7 DNA+100 µM, Lane 8 DNA + 200 µM.
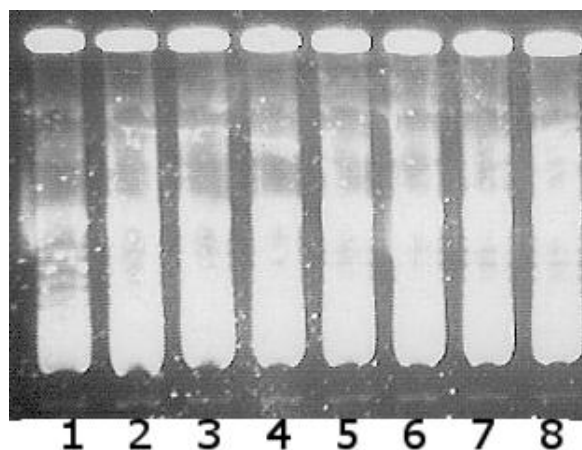
Figure S 7: Agarose gel showing cleavage of DNA (µgµL-1) incubated with diferent concentrations of complex 8. Lane 1 DNA, Lane 2 DNA+10 µM, Lane 3 DNA+20 µM, Lane 4 DNA+30 µM, Lane 5 DNA+40 µM, Lane 6 DNA+50 µM, Lane 7 DNA+100 µM, Lane 8 DNA + 200 µM.
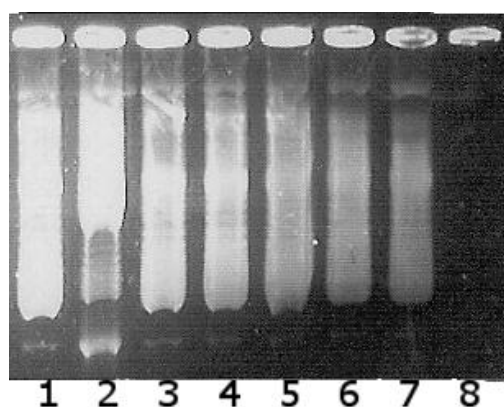
Figure S 8: Agarose gel showing cleavage of DNA (µgµL-1) incubated with diferent concentrations of complex 9. Lane 1 DNA, Lane 2 DNA+10 µM, Lane 3 DNA+20 µM, Lane 4 DNA+30 µM, Lane 5 DNA+40 µM, Lane 6 DNA+50 µM, Lane 7 DNA+100 µM, Lane 8 DNA + 200 µM.

Figure S 9: Agarose gel showing cleavage of DNA (µgµL^{-1}) incubated with diferent concentrations of complex 10. Lane 1 DNA, Lane 2 DNA+10 µM, Lane 3 DNA+20 µM, Lane 4 DNA+30 µM, Lane 5 DNA+40 µM, Lane 6 DNA+50 µM, Lane 7 DNA+100 µM, Lane 8 DNA + 200 µM.

Figure S 10: Agarose gel showing cleavage of DNA (µgµL-1) incubated with diferent concentrations of complex 11. Lane 1 DNA, Lane 2 DNA+10 µM, Lane 3 DNA+20 µM, Lane 4 DNA+30 µM, Lane 5 DNA+40 µM, Lane 6 DNA+50 µM, Lane 7 DNA+100 µM, Lane 8 DNA + 200 µM.
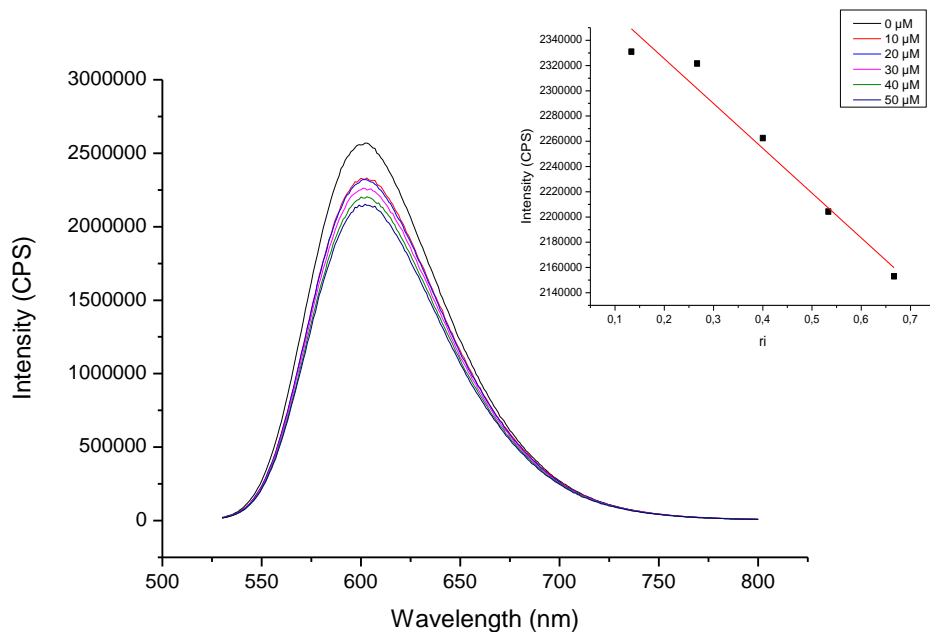
S2. Fluorescence



Figure S 11:Fluorescence quenching curves of EB bound to DNA by complex 1 ([complex] = 0–50 μM). In the graphic showed above is represented the decrease in the maximum intensity vs ri (where ri represents [Complex]/[DNA]).
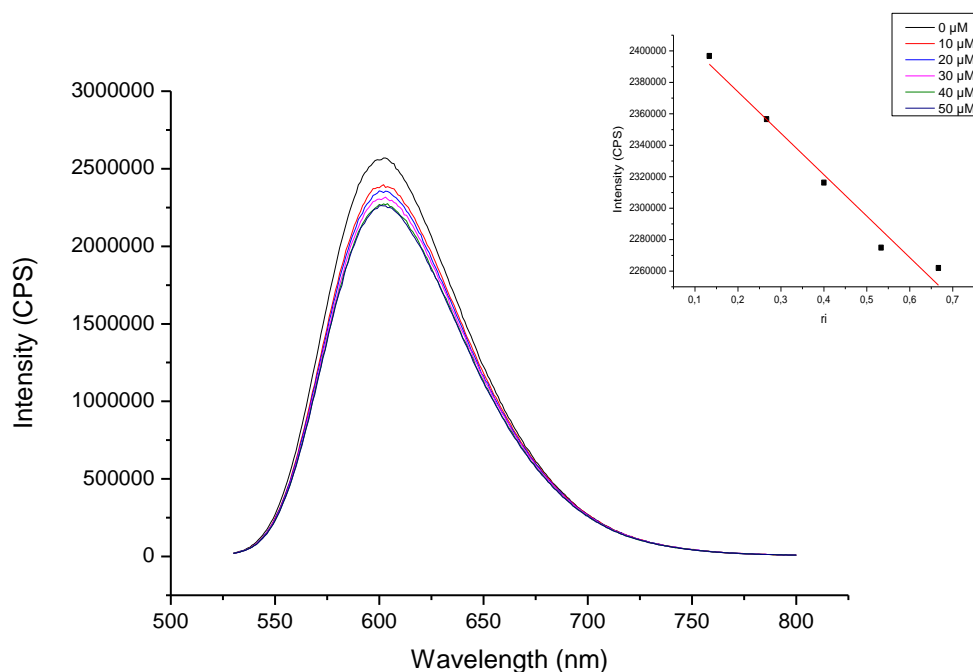
Figure S 12: Fluorescence quenching curves of EB bound to DNA by complex 2 ([complex] = 0–50 μM). In the graphic showed above is represented the decrease in the maximum intensity vs ri (where ri represents [Complex]/[DNA]).
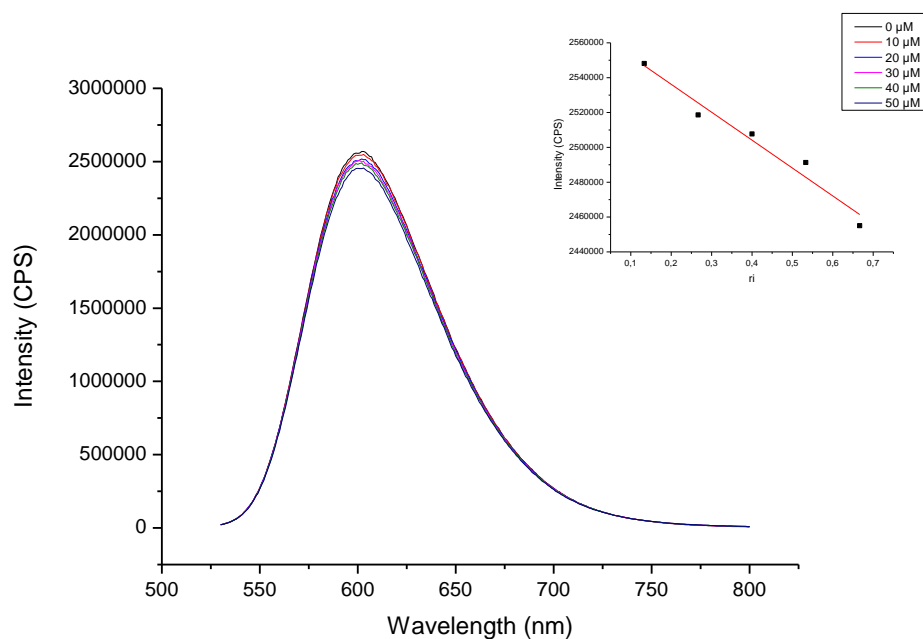
Figure S 13: Fluorescence quenching curves of EB bound to DNA by complex 3 ([complex] = 0–50 µM). In the graphic showed above is represented the decrease in the maximum intensity vs ri (where ri represents [Complex]/[DNA]).
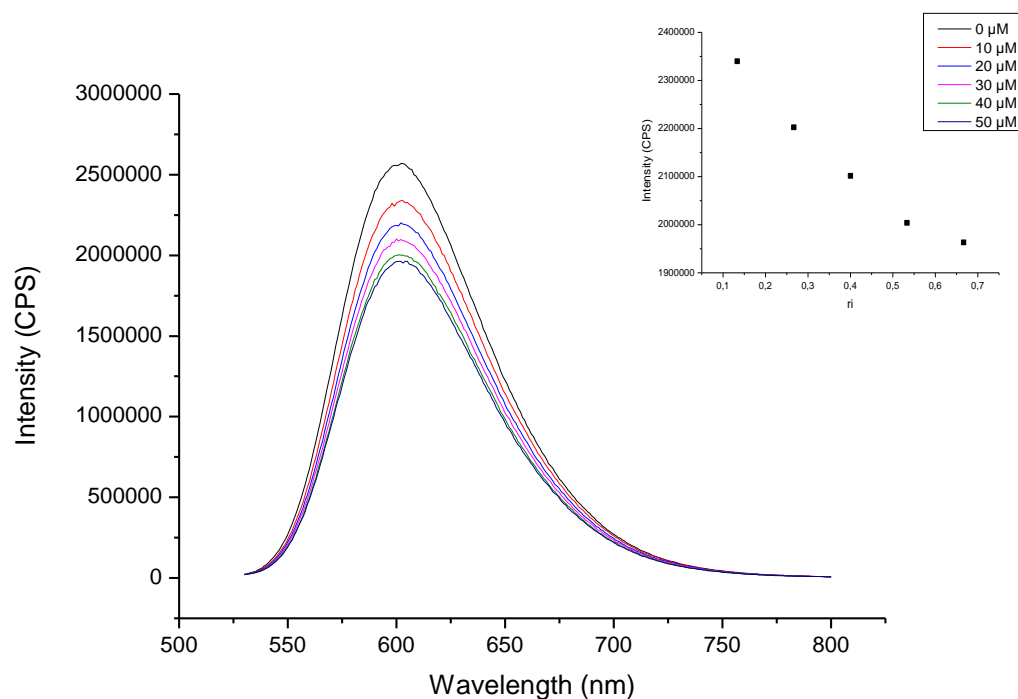
Figure S 14: Fluorescence quenching curves of EB bound to DNA by complex 4 ([complex] = 0–50 µM). In the graphic showed above is represented the decrease in the maximum intensity vs ri (where ri represents [Complex]/[DNA]).
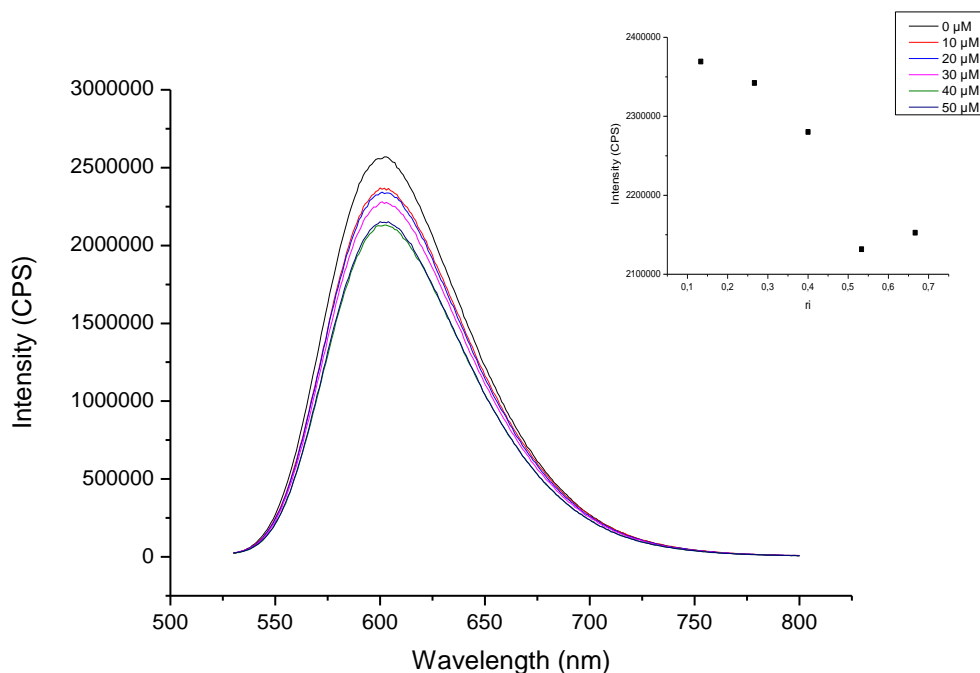
Figure S 15: Fluorescence quenching curves of EB bound to DNA by complex 5 ([complex] = 0–50 μM). In the graphic showed above is represented the decrease in the maximum intensity vs ri (where ri represents [Complex]/[DNA]).
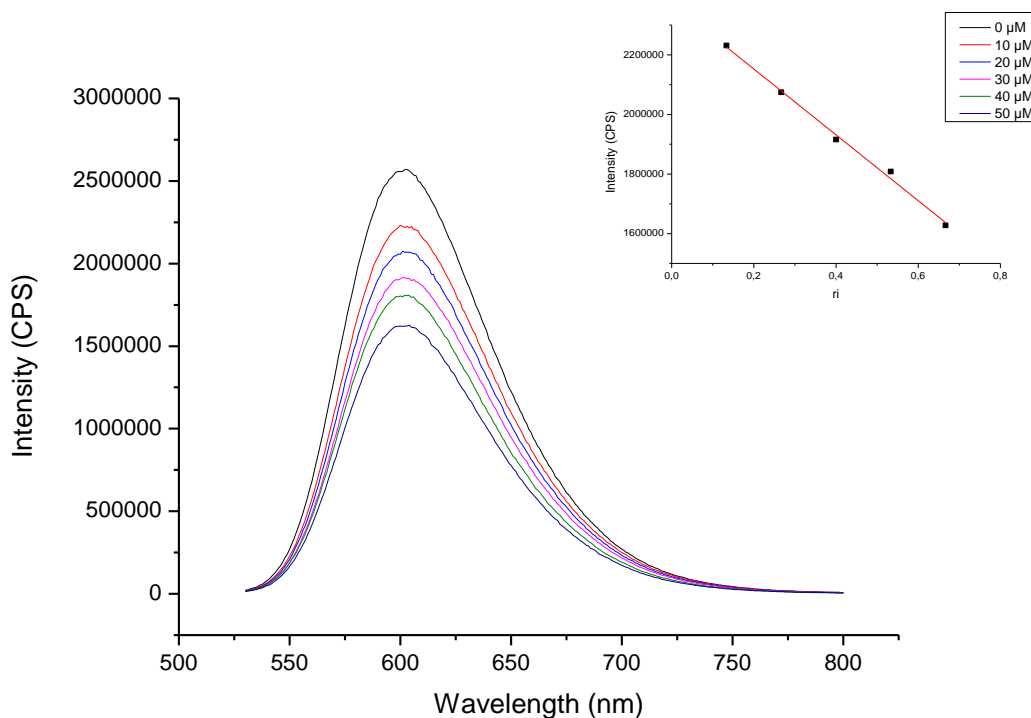
Figure S 16: Fluorescence quenching curves of EB bound to DNA by complex 6 ([complex] = 0–50 μM). In the graphic showed above is represented the decrease in the maximum intensity vs ri (where ri represents [Complex]/[DNA]).
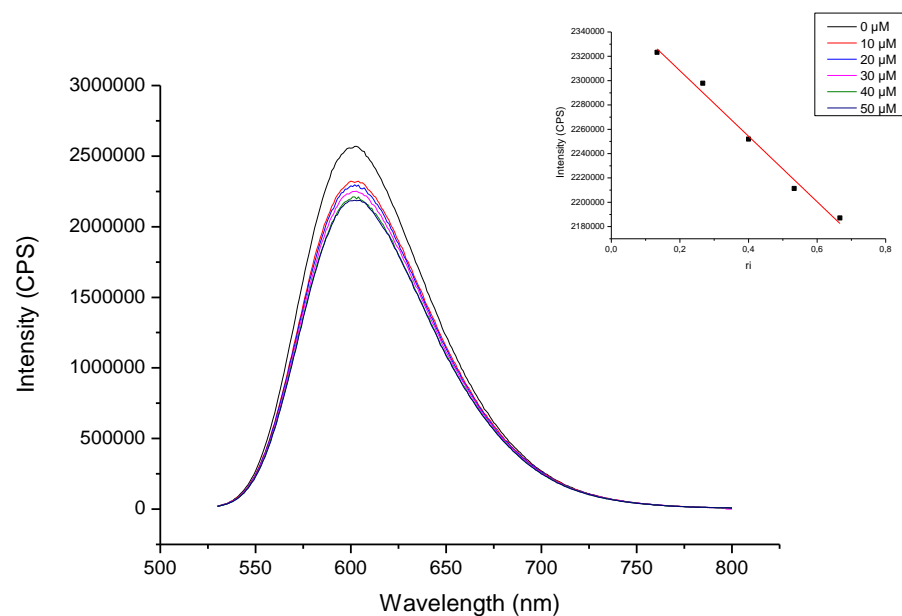
Figure S 17: Fluorescence quenching curves of EB bound to DNA by complex 7 ([complex] = 0–50 µM). In the graphic showed above is represented the decrease in the maximum intensity vs ri (where ri represents [Complex]/[DNA]).
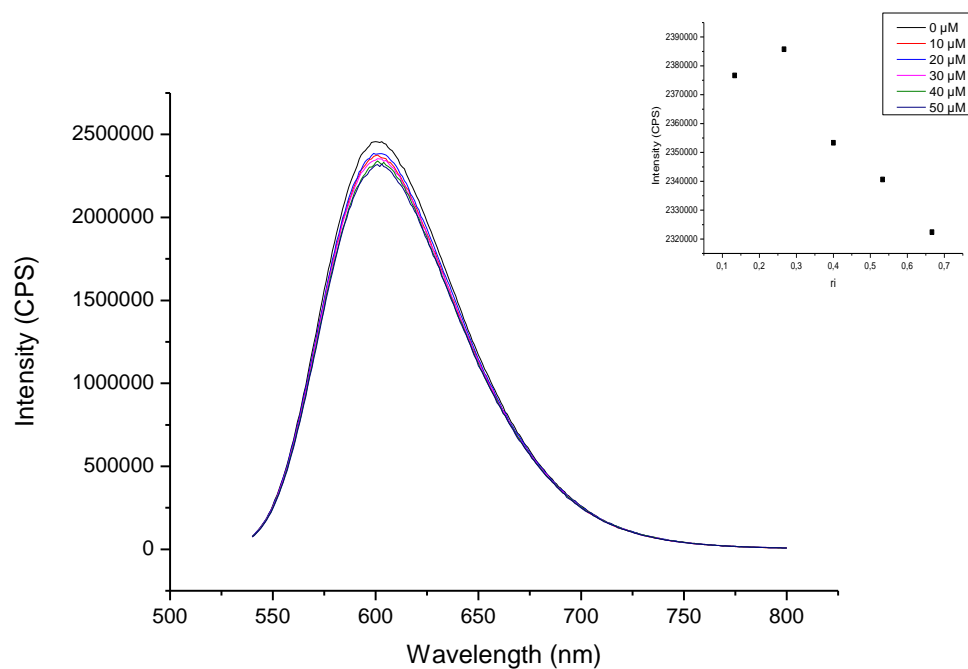
Figure S 18: Fluorescence quenching curves of EB bound to DNA by complex 8 ([complex] = 0–50 µM). In the graphic showed above is represented the decrease in the maximum intensity vs ri (where ri represents [Complex]/[DNA]).
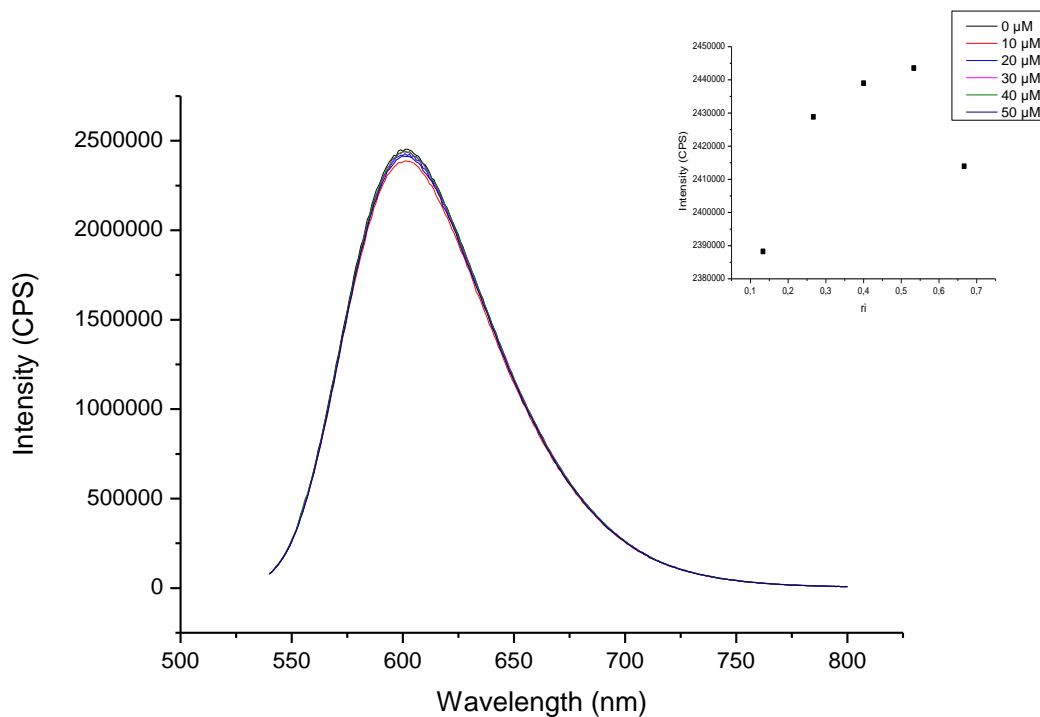
Figure S 19: Fluorescence quenching curves of EB bound to DNA by complex 9 ([complex] = 0–50 µM). In the graphic showed above is represented the decrease in the maximum intensity vs ri (where ri represents [Complex]/[DNA]).
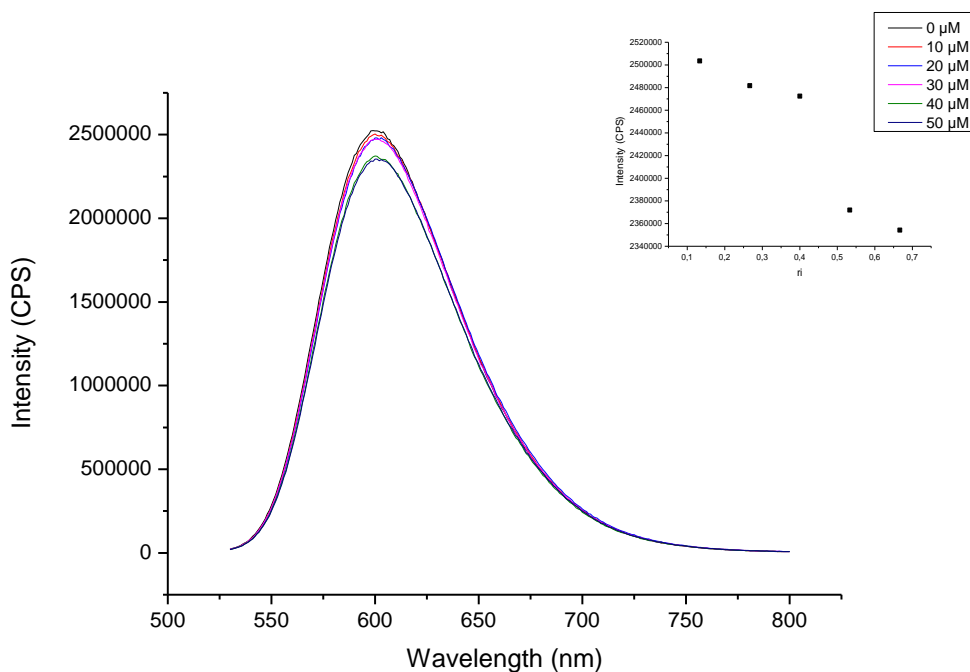
Figure S 20: Fluorescence quenching curves of EB bound to DNA by complex 10 ([complex] = 0–50 µM). In the graphic showed above is represented the decrease in the maximum intensity vs ri (where ri represents [Complex]/[DNA]).
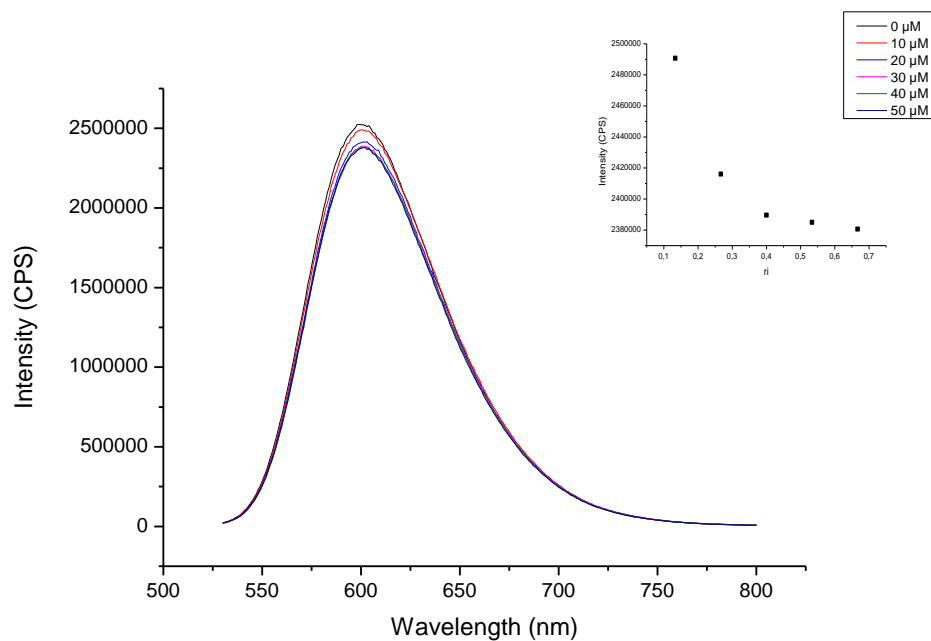
Figure S 21: Fluorescence quenching curves of EB bound to DNA by complex 11 ([complex] = 0–50 μM). In the graphic showed above is represented the decrease in the maximum intensity vs ri (where ri represents [Complex]/[DNA]).

S3. Viscosity results

[Complex]/[DNA]	$(\eta/\eta_0)^{1/3}$ of Copper Complexes						
	Complex 1	Complex 2	Complex 3	Complex 4	Complex 5	Complex 6	Complex 7
0	1	1	1	1	1	1	1
0.33	1.07	1.01	0.99	1.01	0.99	0.96	0.99
0.67	1.05	1.02	1.01	1.02	1.01	0.97	1.01
1.00	1.05	1.08	1.01	1.02	1.02	1.02	1.01
1.33	1.01	1.01	1.03	1.05	1.02	0.99	0.99
1.67	1.01	1.08	1.05	1.08	1.04	1.00	1.02
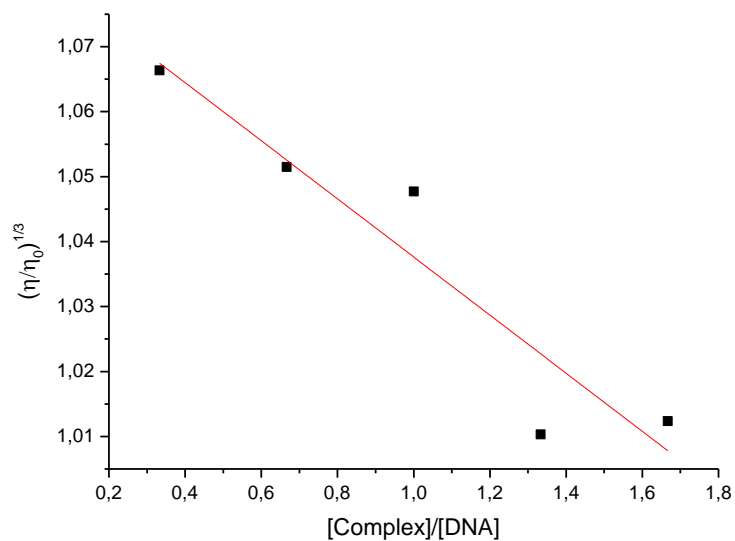
Figure S 22: Alteration on DNA viscosity when incubated 24h with complex 1 with DNA
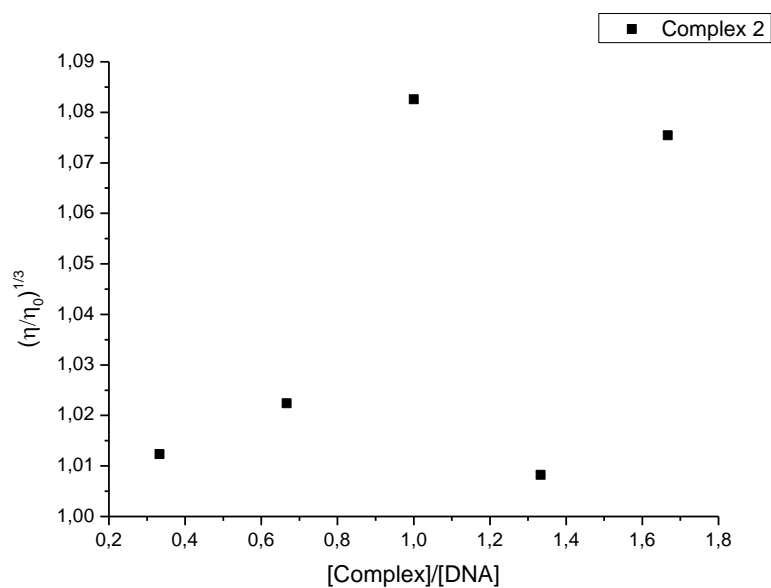
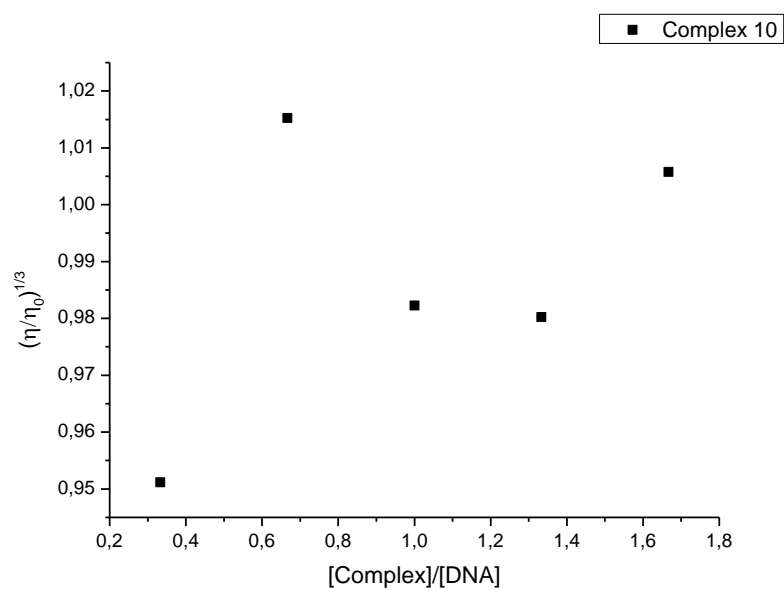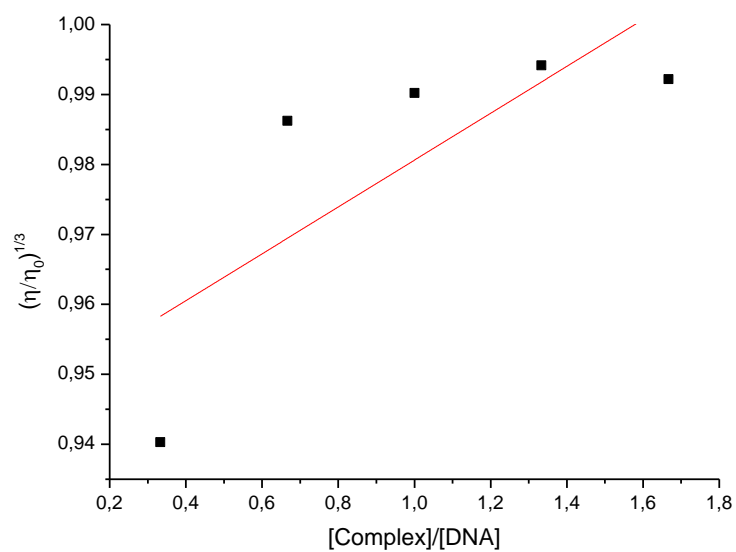**Figure S 23: Alteration on DNA viscosity when incubated 24h with complex 2 with DNA**
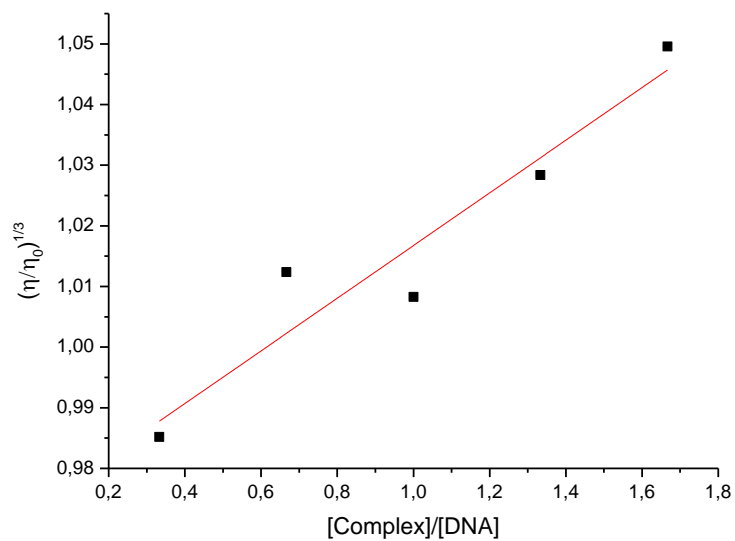
Figure S 24: Alteration on DNA viscosity when incubated 24h with complex 3 with DNA
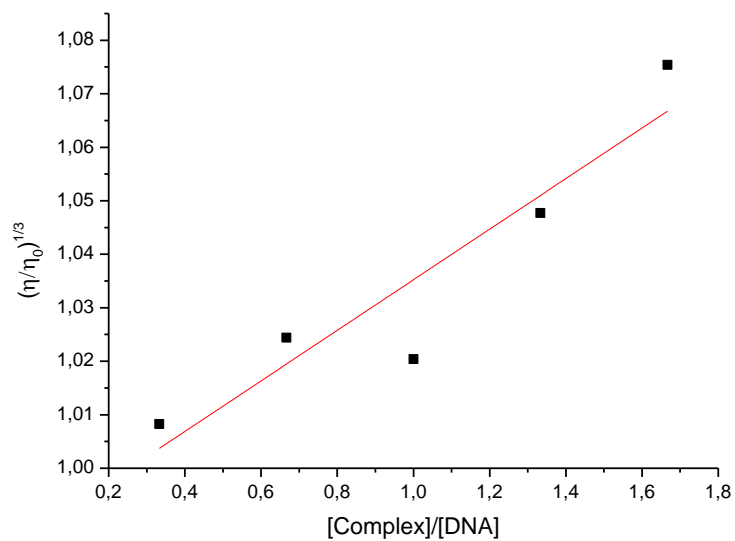
Figure S 25: Alteration on DNA viscosity when incubated 24h with complex 4 with DNA
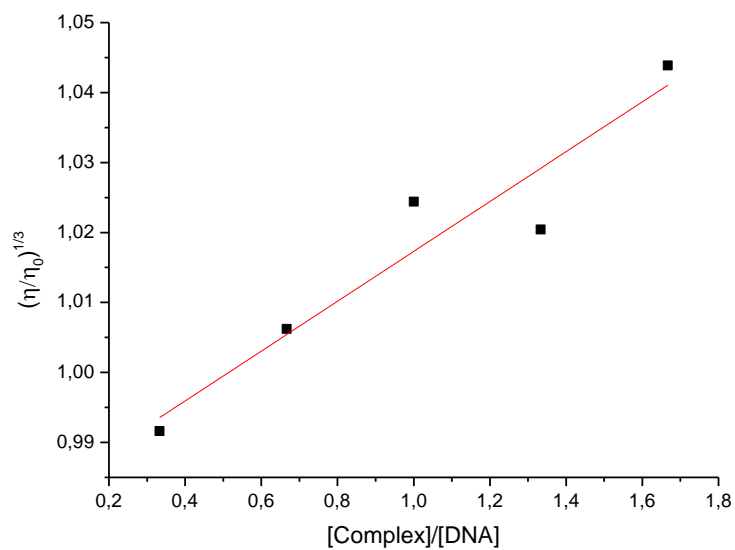
Figure S 26: Alteration on DNA viscosity when incubated 24h with complex 5 with DNA
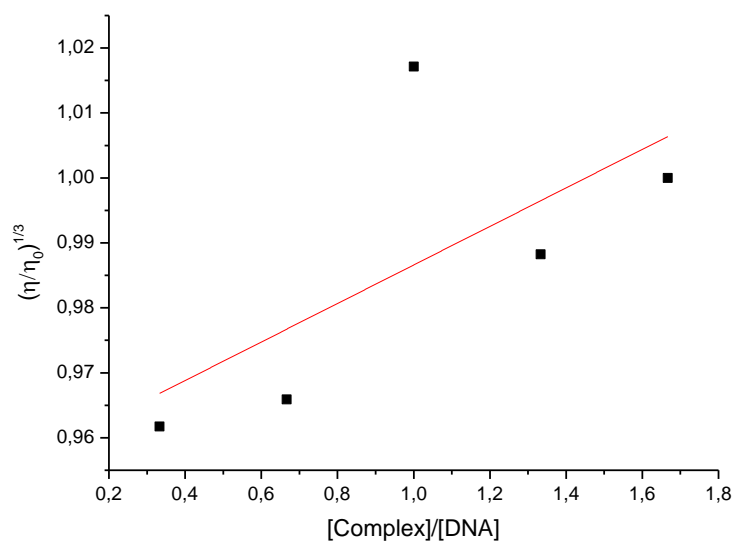
Figure S 27: Alteration on DNA viscosity when incubated 24h with complex 6 with DNA
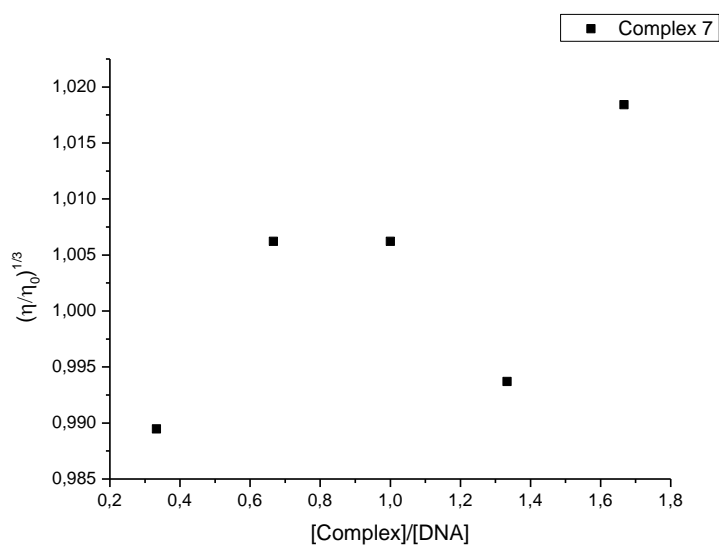
Figure S 28: Alteration on DNA viscosity when incubated 24h with complex 7 with DNA

$(\eta/\eta_0)1/3$ of Zinc Complexes				
[Complex]/[DNA]	Complex 8	Complex 9	Complex 10	Complex 11
0	1	1	1	1
0.33	0.97	0.93	0.95	0.94
0.67	0.97	0.98	1.02	0.99
1.00	0.96	0.97	0.98	0.99
1.33	0.98	1.00	0.98	0.99
1.67	1.04	0.99	1.01	0.99
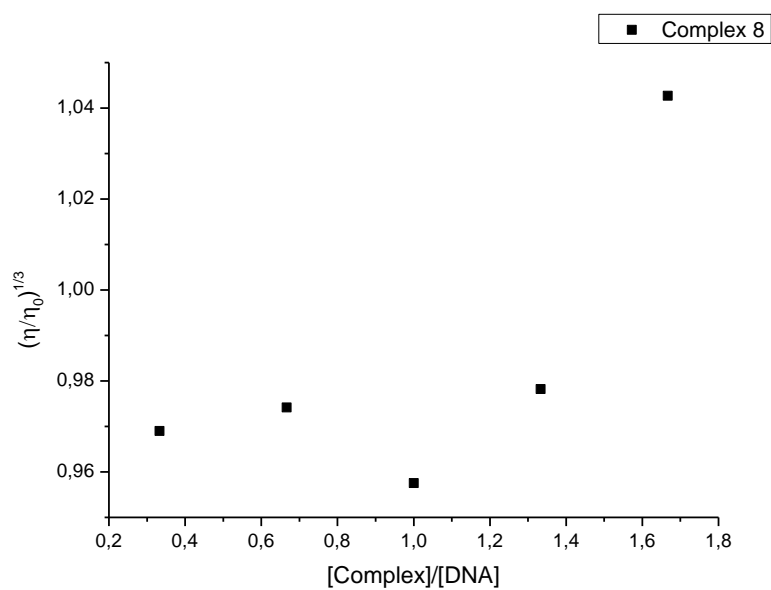
Figure S 29: Alteration on DNA viscosity when incubated 24h with complex 8 with DNA
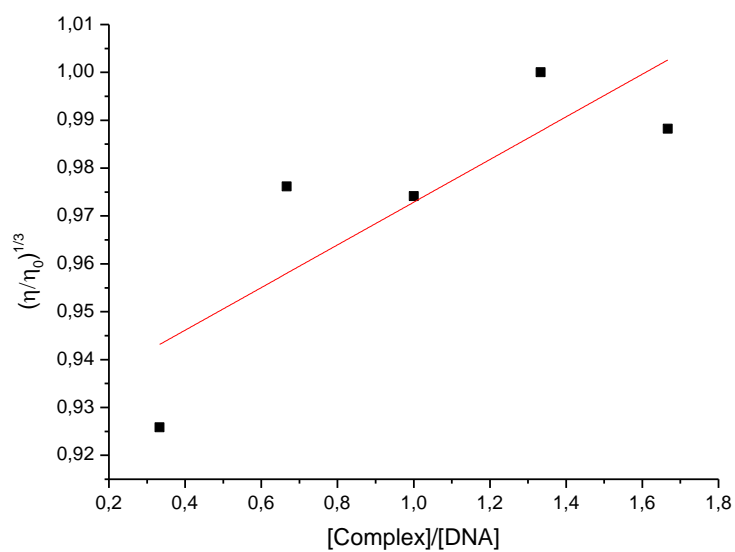
Figure S 30: Alteration on DNA viscosity when incubated 24h with complex 9 with DNA

Figure S 31: Alteration on DNA viscosity when incubated 24h with complex 10 with DNA

Figure S 32Alteration on DNA viscosity when incubated 24h with complex 11 with DNA

S4. AFM Results
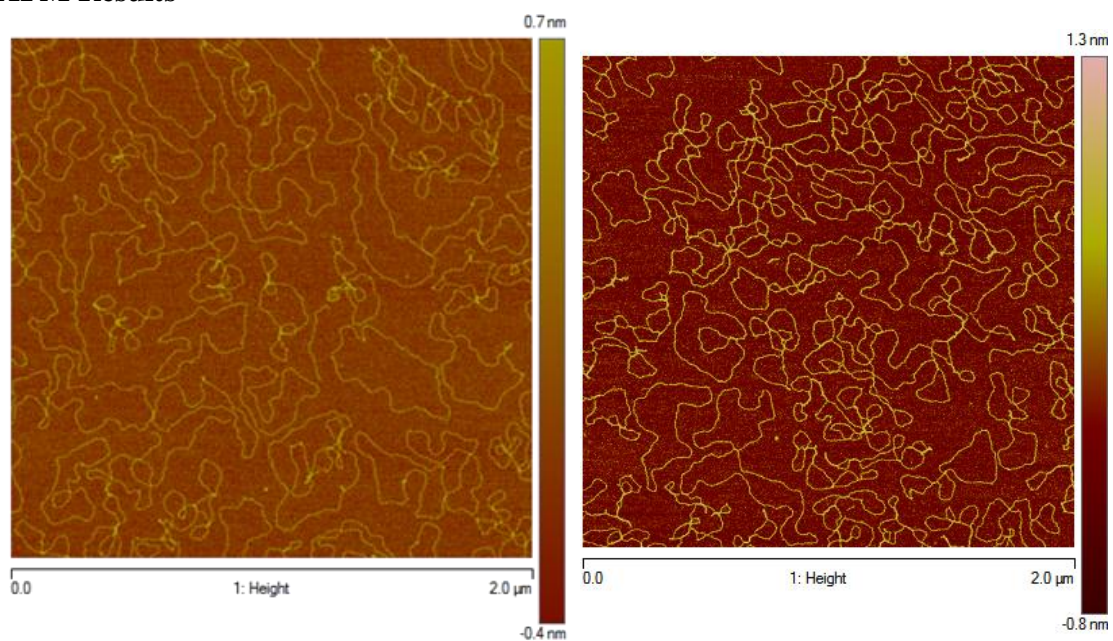
**Figure S 33: AFM image of pBR322 without (left) and with reductant (right)**
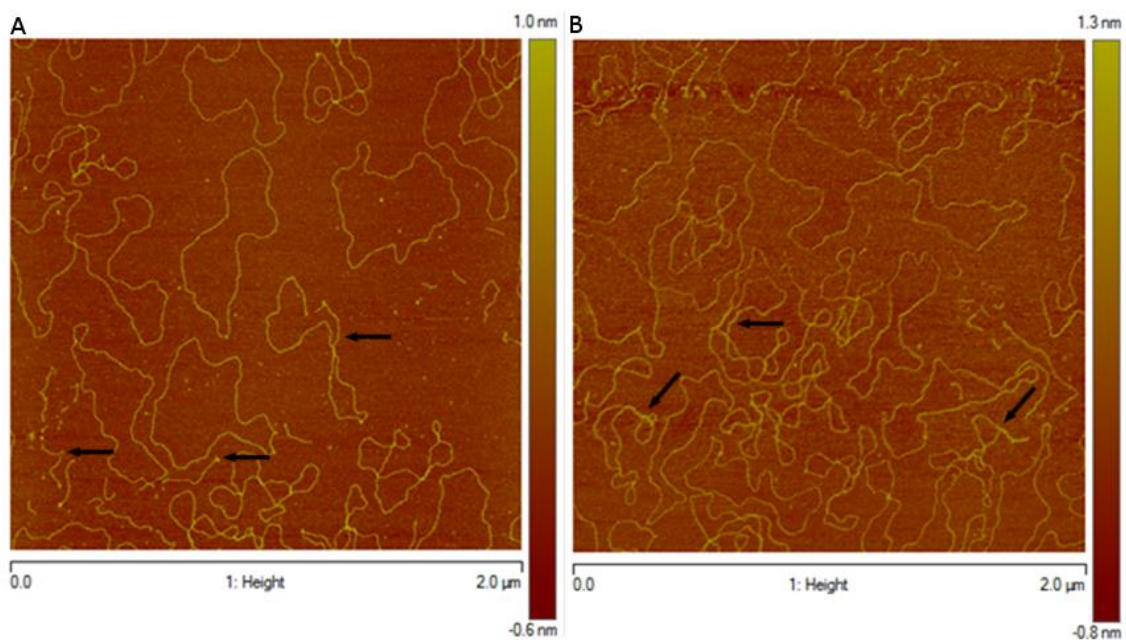
Figure S 34: AFM Image for the interaction of complex 1 and pBR322. In A, the arrows show the nicked form of DNA due to the exposure to 24h incubation. In B the arrows represent some DNA Kinks as mixed toroidal and plectonemic supercoils.
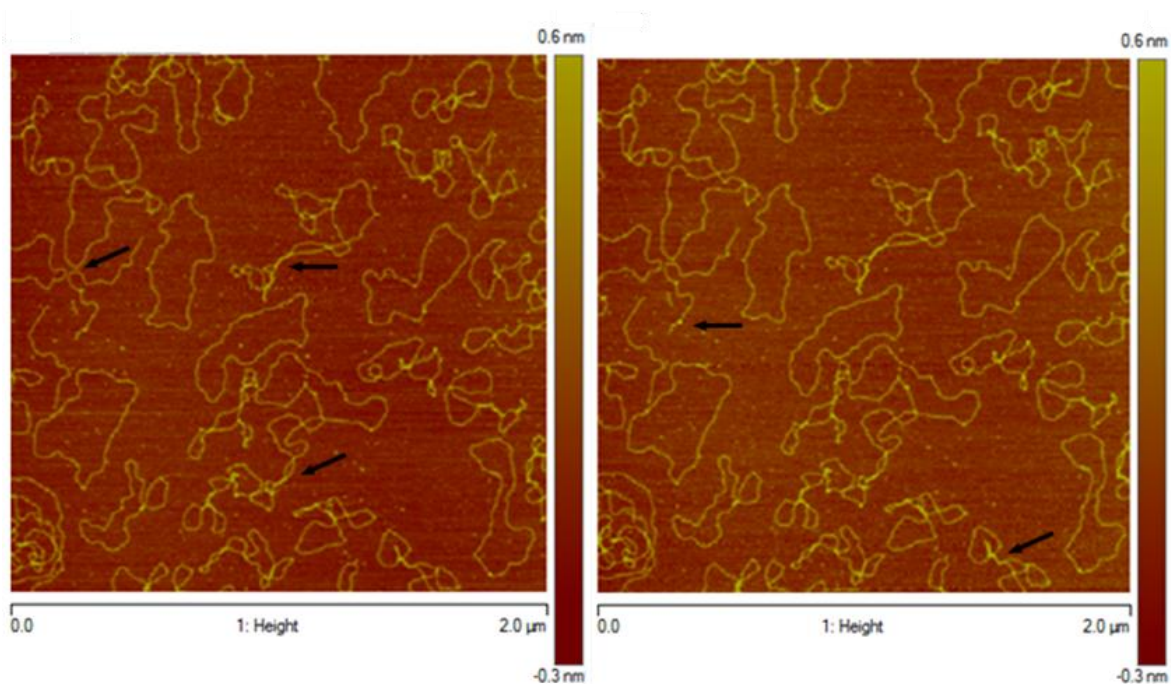
Figure S 35: AFM Image for the interaction of complex 2 and pBR322. The arrows highlight nicked form of DNA some DNA kinks. In this image we can see the relaxed DNA form, the toroidally supercoiled, the mixed toroidal and plectonemic supercoils and the complete plectonemic supercoiling forms.
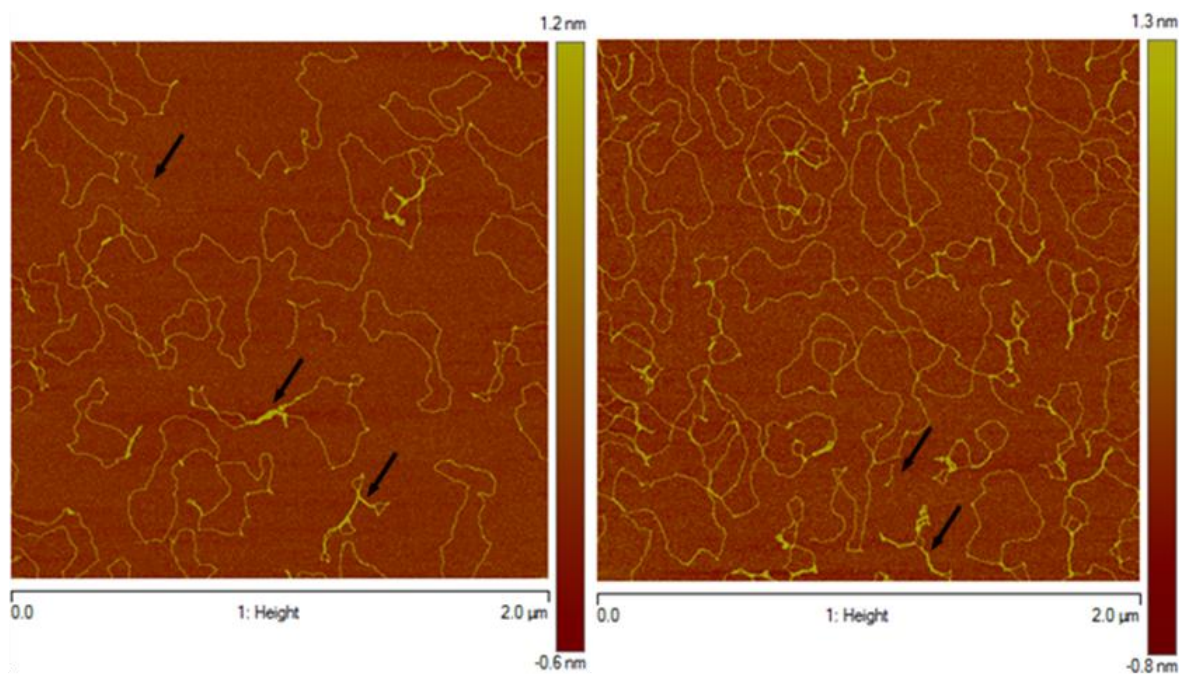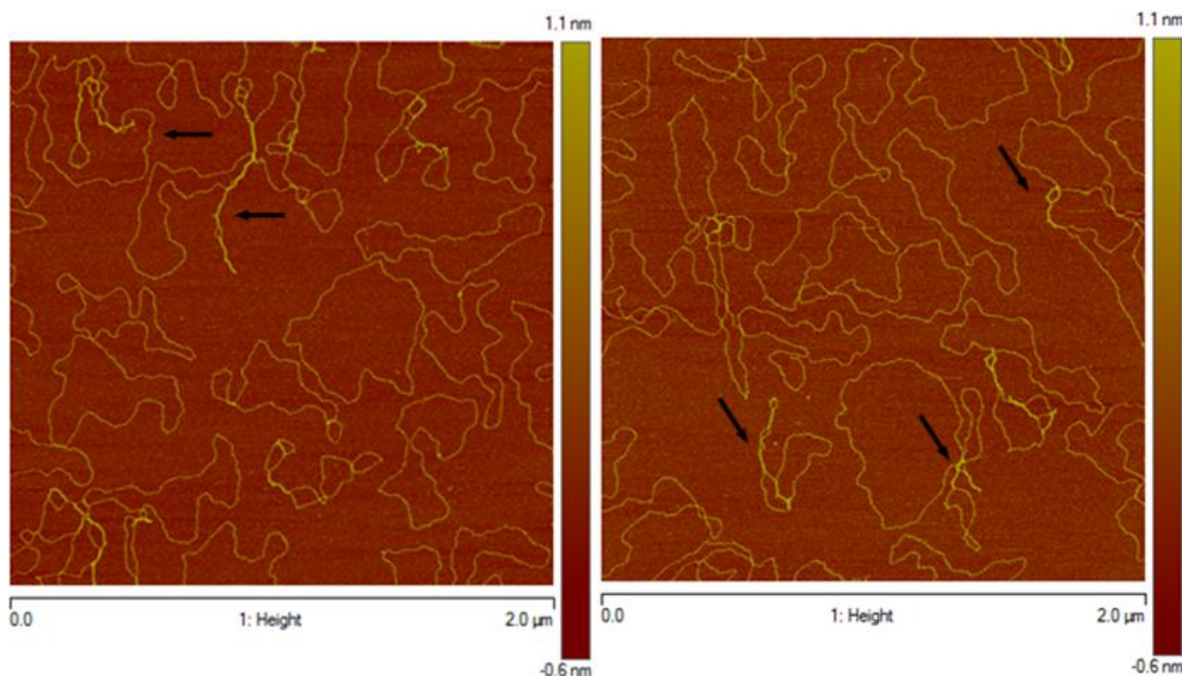

Figure S 36: AFM Image for the interaction of complex 3 and pBR322. The arrows highlight nicked form of DNA some DNA kinks. In this image we can see the toroidally supercoiled, the mixed toroidal and plectonemic supercoils and the complete plectonemic supercoiling forms.
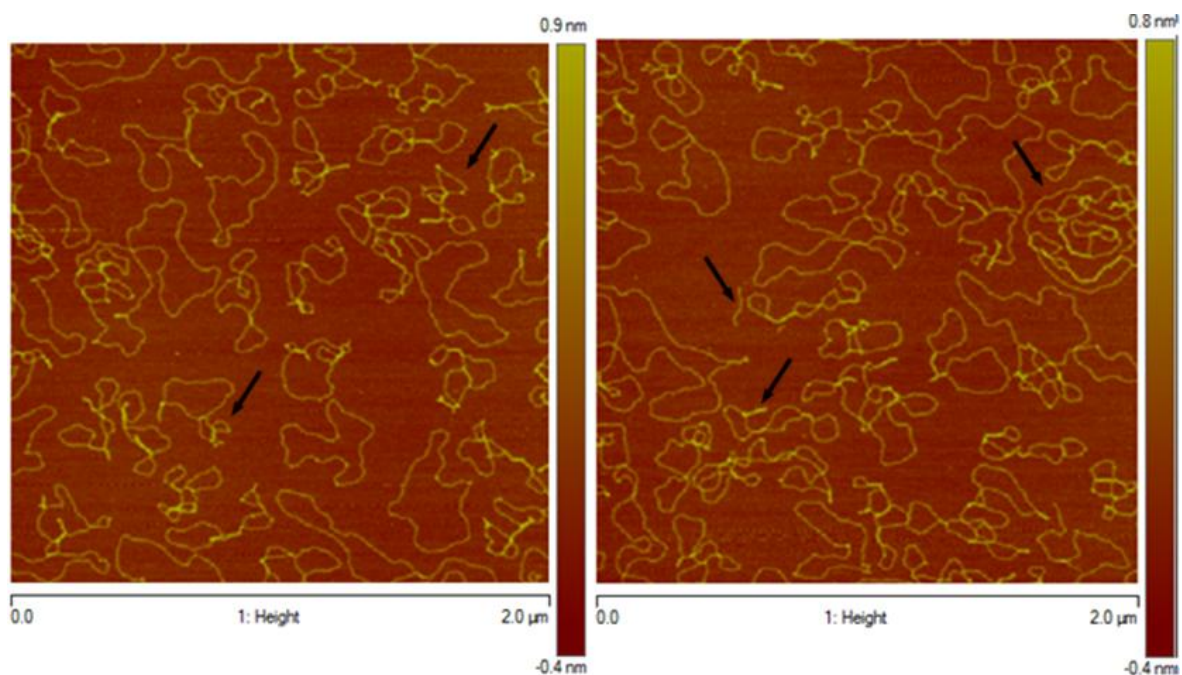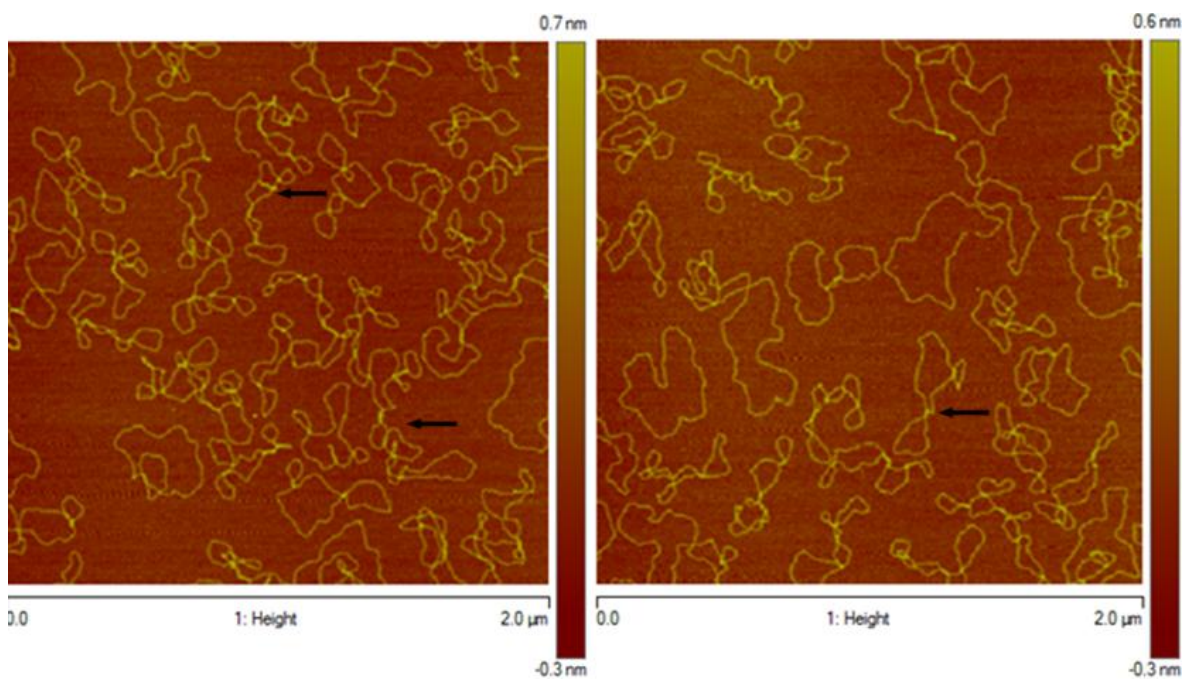
Figure S 37: AFM Image for the interaction of complex 4 and pBR322. The arrows highlight nicked form of DNA some DNA kinks. In this image we can see the toroidally supercoiled, the mixed toroidal and plectonemic supercoils and the complete plectonemic supercoiling forms
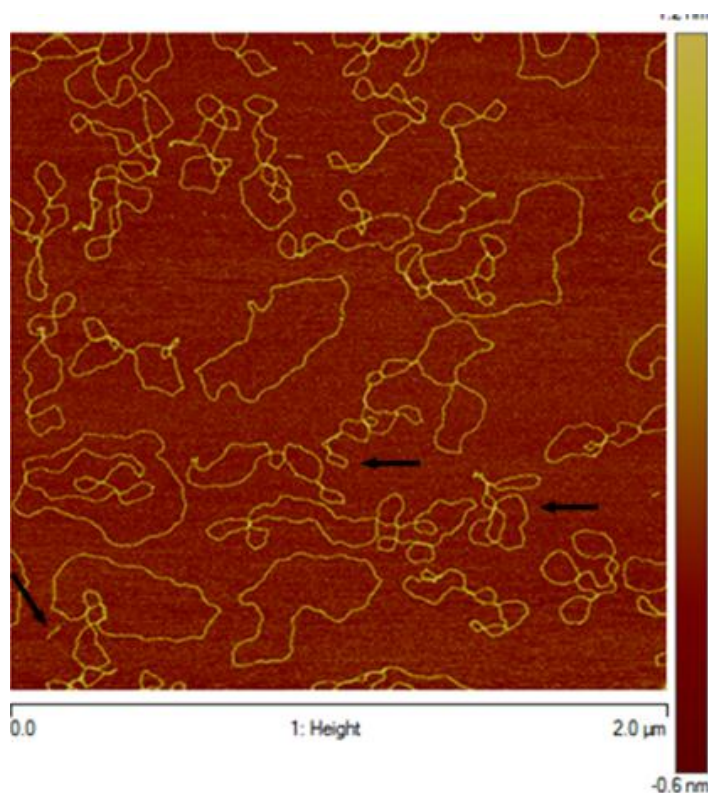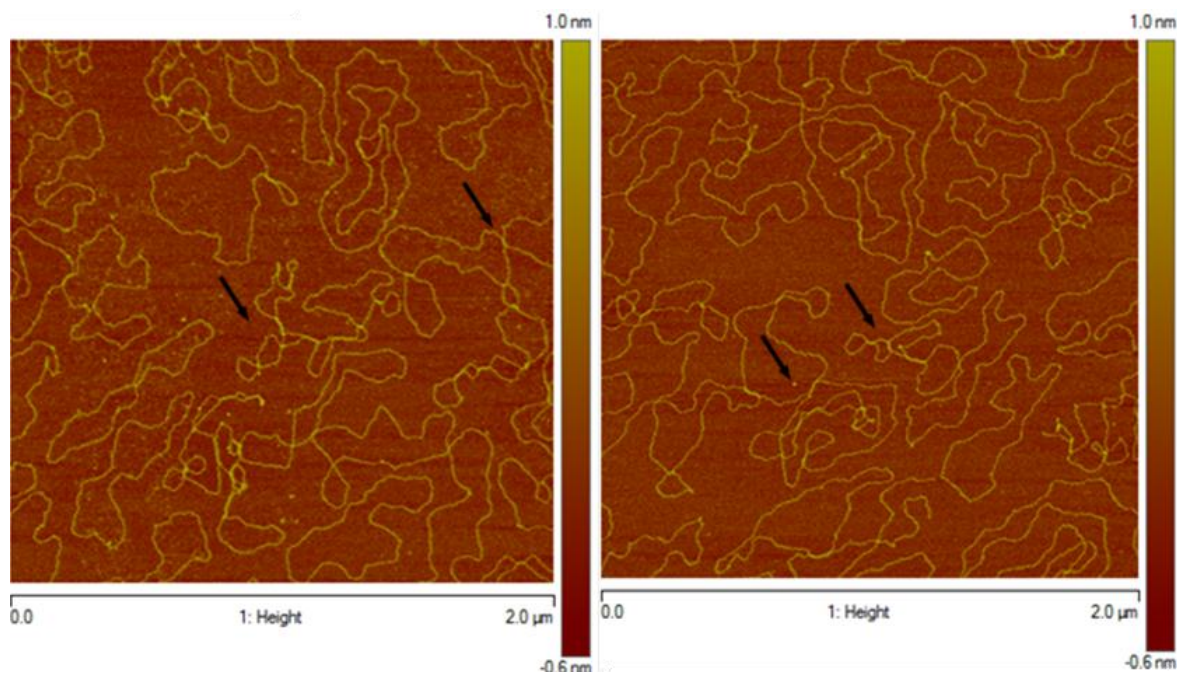

Figure S 38: AFM Image for the interaction of complex 5 and pBR322. The arrows highlight nicked form of DNA some DNA kinks. In this image we can see the toroidally supercoiled, the mixed toroidal and plectonemic supercoils and the complete plectonemic supercoiling forms.

Figure S 39: AFM Image for the interaction of complex 6 and pBR322. The arrows highlight nicked form of DNA some DNA kinks. In this image we can see the toroidally supercoiled, the mixed toroidal and plectonemic supercoils and the complete plectonemic supercoiling forms.
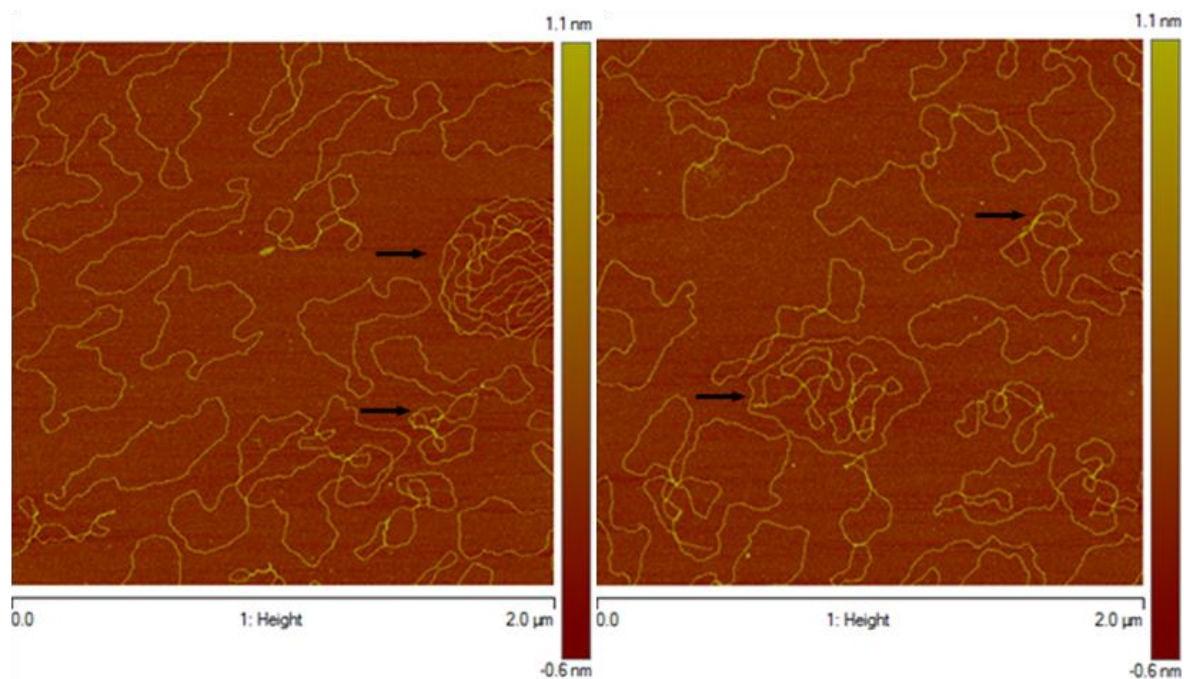

Figure S 40: AFM Image for the interaction of complex 7 and pBR322. The arrows highlight DNA kinks. In this image we can see the toroidally supercoiled, the mixed toroidal and plectonemic supercoils and the complete plectonemic supercoiling forms.

Figure S 41: AFM Image for the interaction of complex 8 and pBR322. The arrows highlight DNA kinks. In this image we can see the toroidally supercoiled, the mixed toroidal and plectonemic supercoils and the complete plectonemic supercoiling forms.
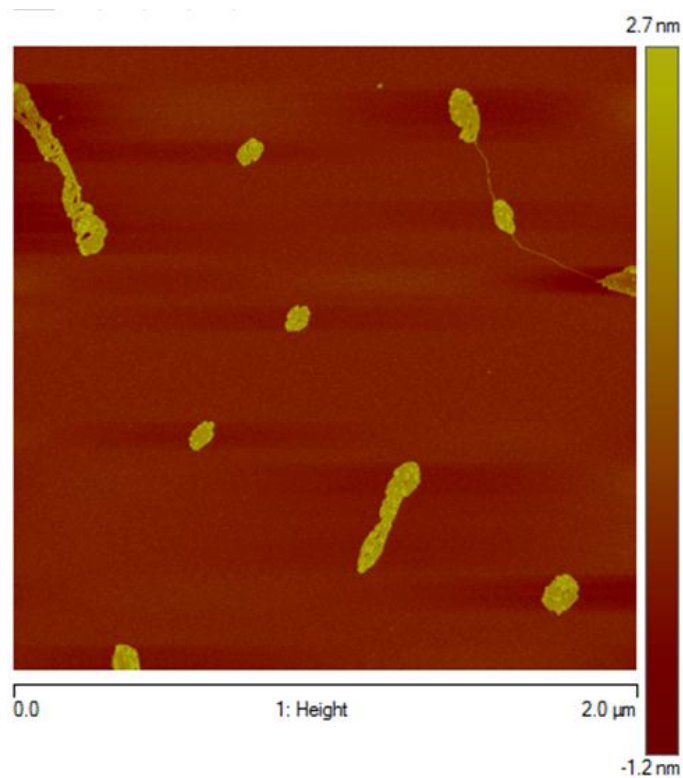

Figure S 42: AFM Image for the interaction of complex 9 and pBR322. The arrows highlight DNA kinks. In this image we can see the toroidally supercoiled, the mixed toroidal and plectonemic supercoils and the complete plectonemic supercoiling forms.

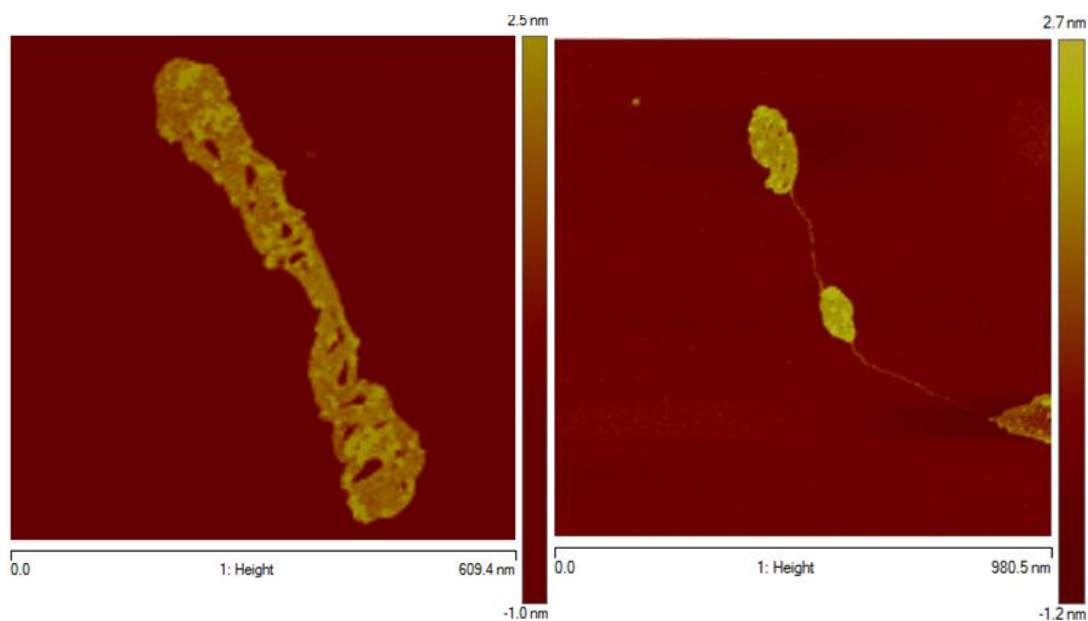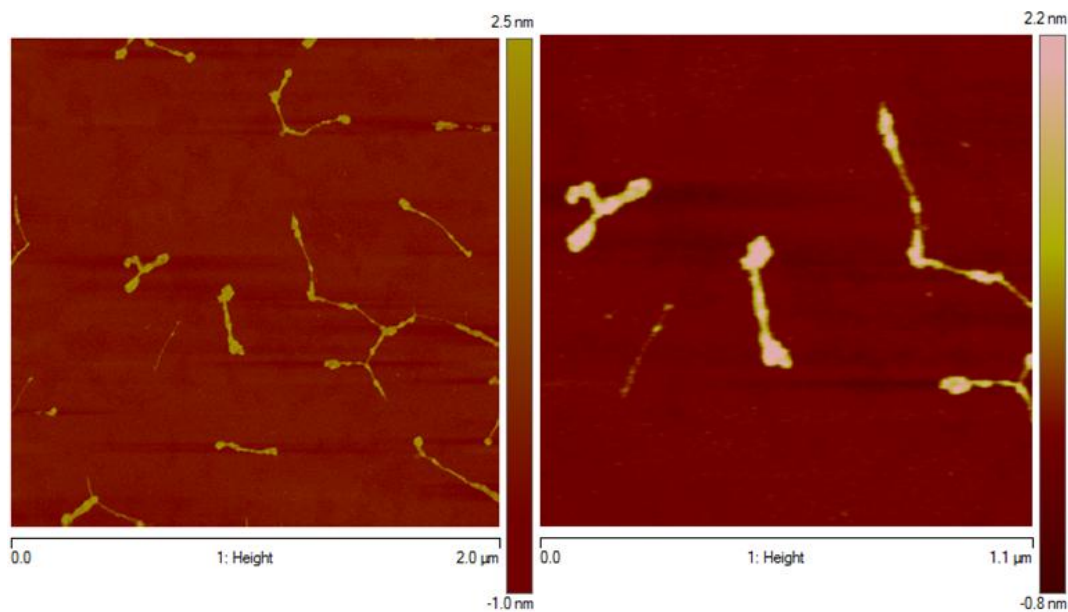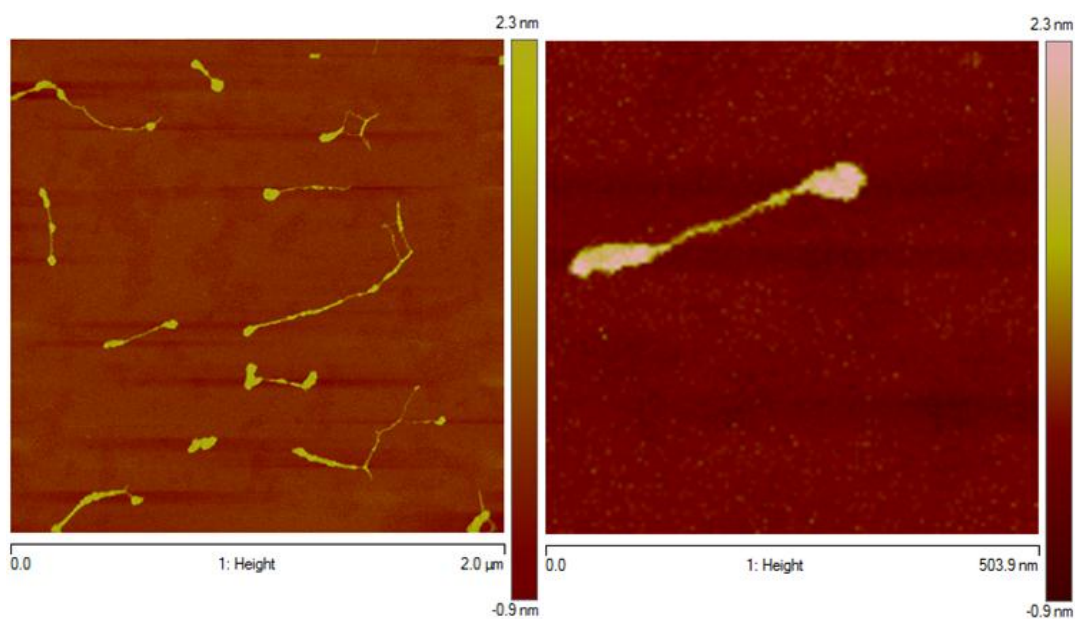**Figure S 43: AFM Image for the interaction of complex 10 and pBR322.**

Figure S 44: Zoom of the previous figure. In these we can perfectly understand the effect of complex 10 when incubated for 24h with pBR322.

Figure S 45: AFM Image for the interaction of complex 11 with DNA, and Zoom of the same image. In these we can perfectly understand the effect of complex 11 when incubated for 24h with pBR322.

Figure S 46: Another AFM Image for the interaction of complex 11 with DNA, and Zoom of the same image. In these we can perfectly understand the effect of complex 11 when incubated for 24h with pBR322.